4.2.7 Precambrian Rocks

The Precambrian rocks underlying Permian formations contain very limited amounts of groundwater. In the Zuni Mountains, groundwater in these rocks is occasionally encountered in saturated faults or fracture zones (Baldwin and Rankin 1995). Alternatively, limited amounts of subsurface water are sometimes present in weathered material within the uppermost 200 to 300 ft of Precambrian rock. In areas that are not faulted or fractured, the hydraulic conductivity of the rocks is very small, and virtually no water is transmitted.

4.3 Regional Groundwater Flow System

4.3.1 Recharge and Discharge

4.3.1.1 Alluvial Aquifer

Under natural conditions, recharge to the alluvial aquifer is from direct precipitation on the alluvium, direct precipitation on the Bluewater Basalt that quickly seeps through the basalt to underlying alluvium, seepage losses from streams and other surface water features, infiltration of occasional surface water flow during and after storm events, and upward leakage from the San Andres aquifer where its hydraulic heads are larger than those in overlying alluvium. Additional sources of recharge were created when settlers began to populate the Grants-Bluewater Valley. The anthropogenic sources of subsurface water included seepage of water from irrigation canals and infiltration of irrigation water applied to the land surface.

Though mill-related forms of recharge, such as downward seepage of water from the main tailings impoundment, appeared to occur in earlier years at the Bluewater site, this form of recharge appears to have declined greatly since injection of tailings waste fluid began in 1960. Recharge from downward seepage of tailings fluids has decreased even more since site decommissioning in the 1990s.

Groundwater levels in the alluvial aquifer suggest that direct recharge to the aquifer from stream seepage occurs along a reach of Bluewater Creek that extends about 0.5 mi south from the mouth of Bluewater Canyon to the irrigation diversion structure (Figure 3). When flows in Bluewater Creek are sufficiently large to allow flow in the creek channel downstream of the diversion structure, recharge to the alluvial aquifer from creek seepage losses also likely takes place. This also holds true for the Rio San Jose channel downstream of the confluence of Bluewater Creek and Mitchell Draw. Occasionally, streamflow downstream of the diversion structure is large enough to deliver surface water to an abandoned borrow pit located directly south of the Bluewater site (Figure 3), in an area just south of Highway 122 and directly west of Bluewater production wells Anaconda #3 and Anaconda #4 (Figure 4 and Figure 16). The borrow pit is considered a recharge source (Hydro-Search 1981a, Frenzel 1992), as are reaches of the Rio San Jose downstream of the pit when flows in the river are high enough to deliver water that far downstream. In addition to seepage from Bluewater Creek and the Rio San Jose, surface water losses from irrigation canals contribute substantially to the alluvial aquifer downstream of the major diversion structure on Bluewater Creek.

Under natural conditions, recharge to the alluvial aquifer due to upward leakage from the San Andres aquifer tends to occur in an irregularly shaped area extending from about 1 mile north of Toltec to Grants. Upward flow from the bedrock aquifer is possible here because the Chinle Formation is absent, so that the alluvial aquifer directly overlies the San Andres Limestone.

Upward hydraulic gradients from the bedrock aquifer to the alluvium are created in this area because of accumulating recharge to the San Andres aquifer from precipitation on the nearby Zuni Mountains.

Recharge to the alluvium on the east end of the Grants-Bluewater Valley can be attributed to injection wells and trenches used by HMC on the south end of the Homestake site. In addition, irrigation conducted by HMC on land south and west of the large tailings disposal cell as part of the GRP contributes recharge to the alluvial aquifer.

Though not specifically called recharge, a large amount of alluvial aquifer flow in the Grants-Bluewater Valley is attributed to groundwater inflow from areas bordering the study area. Such subsurface inflow occurs along a 3-mile stretch of the study area's north boundary that lies north-northwest of the Bluewater site. Subsurface inflow to the alluvial aquifer also occurs in the northeast corner of the study area via south-southwestward-migrating groundwater in San Mateo Creek alluvium.

Discharge from the alluvial aquifer takes place through various mechanisms. Much of it is attributed to evapotranspiration in agricultural areas and groundwater withdrawal by wells. Downward leakage of alluvial aquifer groundwater to the San Andres aquifer is also possible in areas where hydraulic heads in the former are larger than underlying heads in the San Andres aquifer. Such downward gradients occur in the recent Rio San Jose alluvium between the mouth of Bluewater Canyon and about 4 mi downstream of the irrigation diversion structure. In addition, downward groundwater migration from the alluvial aquifer to the San Andres aquifer via a branch of the San Mateo Fault has been mentioned as a possibility at the GRP (EPA 2011) despite the local presence of 500 ft or more of the Chinle Formation between the two aquifers. Downward seepage of groundwater into the San Andres aquifer appears to occur in the vicinity of Milan's northernmost municipal wells because pumping of the wells caused a reversal of the local vertical hydraulic gradient.

Discharge of groundwater from the alluvial aquifer to streams in the Grants-Bluewater Valley is minimal to nonexistent. An area where such discharge is known to occur is the Rio San Jose at Horace Springs, which is east of Grants and beyond the east boundary of the study area.

4.3.1.2 San Andres Aquifer

Recharge to the San Andres aquifer occurs on outcrops of sandstone and limestone in the Zuni Mountains southwest of the Grants-Bluewater Valley, by either direct precipitation on or surface water flow across rock outcrops. This type of recharge also occurs along the east side of the Zuni Mountains, above San Rafael. Frenzel (1992) identified five different recharge zones in the Zuni Mountains, three of which affect the San Andres aquifer in the study area. Two of the recharge zones lie within the study area, and the third is located west of the study area's west boundary, in an area south of Bluewater Lake. As part of a groundwater modeling study, Frenzel (1992) developed temporally varied recharge rates for the recharge zones for the water years 1932 to 1985. The method employed for this purpose was quite detailed and involved cumulative precipitation totals for each 6-month period during the 54 water years. The methods employed to estimate these time-varying recharge quantities on the Zuni Mountains are beyond the scope of this conceptual modeling study. The average recharge flux from this recharge source was about 0.1 cfs, or 44.8 gpm, per mile of mountain front.

Another major source of recharge to the San Andres aquifer originates as leakage of water from Bluewater Lake (Frenzel 1992), which enters outcrops of San Andres aquifer rock. This recharge first occurred around the start of the 20th century due to the presence of an earthen dam that created the lake, and it has occurred regularly since 1927, when a concrete dam was constructed to hold the lake water. The manner in which the leaked lake water ends up as recharged groundwater in the aquifer is complex, as some of the leakage flows back into Bluewater Creek just downstream from the dam (Frenzel 1992). Despite this return flow to the creek, net inflow to the San Andres aquifer from Bluewater Lake leakage is large and a major source of recharge in the Grants-Bluewater Valley.

In addition to the recharge from sources on the Zuni Mountains, subsurface inflow along the north boundary of the study area likely contributes to groundwater flow in the San Andres aquifer. It is difficult to assess this groundwater source, however, because most equipotentials for the aquifer trend north-south in the vicinity of the north boundary, indicating that flow here is directly to the east rather than to the southeast.

A large amount of the discharge from the San Andres aquifer occurs in the form of groundwater extraction for agricultural, municipal, and commercial purposes. Additional outflow is attributed to spring discharge and upward leakage into the alluvial aquifer, particularly in areas where the Chinle Formation is absent. Historically, a large amount of discharge from the San Andres aquifer was attributed to spring discharge at Ojo del Gallo near the San Rafael Fault.

Evapotranspiration from the San Andres aquifer is considered to be a minor form of aquifer discharge in this study. Equipotentials for the aquifer in the easternmost third of the Grants-Bluewater Valley suggest that subsurface outflow across the east boundary of the study area constitutes a large amount of aquifer discharge. A lesser amount of subsurface outflow appears to take place across the south boundary of the study area south of Grants.

4.3.2 Information Sources Relevant to Groundwater Flow

Groundwater flow in the alluvial and San Andres aquifers was analyzed using water level data from wells screened in each of the aquifers. Several different information sources were accessed to gather these data, beginning with consultant reports on the hydrology of the Bluewater site in the late 1970s (Hydro-Search 1977, 1978, 1981a). More recent water level data were derived from monitoring reports by additional consultants and ARCO through the mid-1990s. DOE has been collecting groundwater level data at multiple locations since 1997. Additional water level data for wells monitored by HMC in the east half of the Grant-Bluewater Valley have been tabulated in annual monitoring reports for the Homestake site (e.g., HMC and Hydro-Engineering 2013). Historical water level data dating back to the 1940s are also available for 13 wells in the Grants-Bluewater Valley that USGS has monitored and continues to monitor.

Data from the above-mentioned information sources were used to establish a network of wells in the Grants-Bluewater Valley in this study for the purpose of compiling water level and water chemistry data that assist in developing a regional conceptual model. The locations of the wells that make up the network are shown in Figure 16 through Figure 19 for four sub-areas within the entire study area. Plate 7 presents a single map showing all well locations. Because the monitoring locations were drawn from a variety of studies, several of the wells are identified by more than one label. Appendix B presents a list of all monitoring locations, their spatial coordinates, and a cross-reference of all the labels used to identify the wells.

4.3.3 Potentiometric Surfaces

Groundwater flow in the ancestral and recent river deposits within the alluvial aquifer is generally in the same direction as surface water flow in the Rio San Jose drainage. Water moves southward in the alluvium from where the aquifer crosses the north boundary of the study area, then turns to the southeast and east-southeast in the area where Bluewater Creek discharges from Bluewater Canyon and contributes recharge to the aquifer. Groundwater in the San Mateo Creek alluvium, migrating southwest, merges with Rio San Jose alluvial groundwater at multiple locations north of Milan. As part of a study of regional groundwater flow, Hydro-Search (1981a) developed a potentiometric surface for the alluvial aquifer based on water level data collected at several wells in 1980. A slightly modified version of the surface, presented in Figure 20, illustrates flow directions in the alluvial aquifer under hydrologic conditions that existed more than 30 years ago.

A more recent illustration of groundwater levels in the alluvial aquifer was developed by coupling water elevation data collected by DOE at monitoring wells on and near the Bluewater site with alluvial aquifer water level data published by HMC for the GRP in 2012 (HMC and Hydro-Engineering 2013). The results of this latter effort, presented in Figure 21, suggest that groundwater levels in 2012 in the vicinity of the Bluewater site were, on average, slightly lower than those observed in 1980. In contrast, groundwater levels in the vicinity of the GRP appear to have been slightly higher in 2012 than in 1980.

The use of water elevation data from the GRP to prepare Figure 21 provides insight into groundwater flow in ancestral Rio San Jose alluvium in areas outside the Bluewater site. Water level data from seven wells monitored by HMC assist in discerning the flow direction in offsite areas as well as the location of a distinct paleochannel in the ancestral river alluvium. The interpretation resulting from the combined data sets, as expressed by water elevation contours in Figure 21, suggests that the paleochannel extends about 1 mi southeastward from the southeast corner of the Bluewater site before merging with San Mateo Creek alluvium. Bluewater-site wells T(M), 22(M), X(M), and 21(M) appear to lie within the paleochannel, as do GRP wells 636, 637, and 686 in offsite areas (Figure 21).

In addition to providing information regarding flows in the ancestral river alluvium, Figure 21 reveals that conceptualization of groundwater pathways and flow directions in the San Mateo Creek alluvium has changed somewhat over the past 30 years. To better illustrate those changes, a separate map showing measured hydraulic heads in the alluvial aquifer in the vicinity of the Homestake site, as modified from a map included in an annual GRP report (HMC and Hydro-Engineering 2013), is reproduced in Figure 22. This figure shows that the most obvious change in the alluvial aquifer potentiometric surface in recent years is observed in an area about 1.5 mi southwest of the Homestake site's large tailings disposal cell. Monitoring data from this area indicate that groundwater flows around either end of a 2 mi long, buried bedrock ridge of the Chinle Formation, or bedrock high, in the base of the aquifer. This observation in turn signifies that flow in the San Mateo Creek alluvium merges with flow in Rio San Jose alluvium at two separate locations (Figure 21 and Figure 22). The first location is about 1 mi southeast of the Bluewater site, as discussed in the previous paragraph. The second location is about 2 mi south-southwest of the large tailings disposal cell at the Homestake site and approximately 1.5 mi directly east of Toltec. This updated conceptualization affects the interpretation of how contaminant plumes in the ancestral Rio San Jose alluvium originating at the Bluewater site merge with those migrating from the Homestake site.

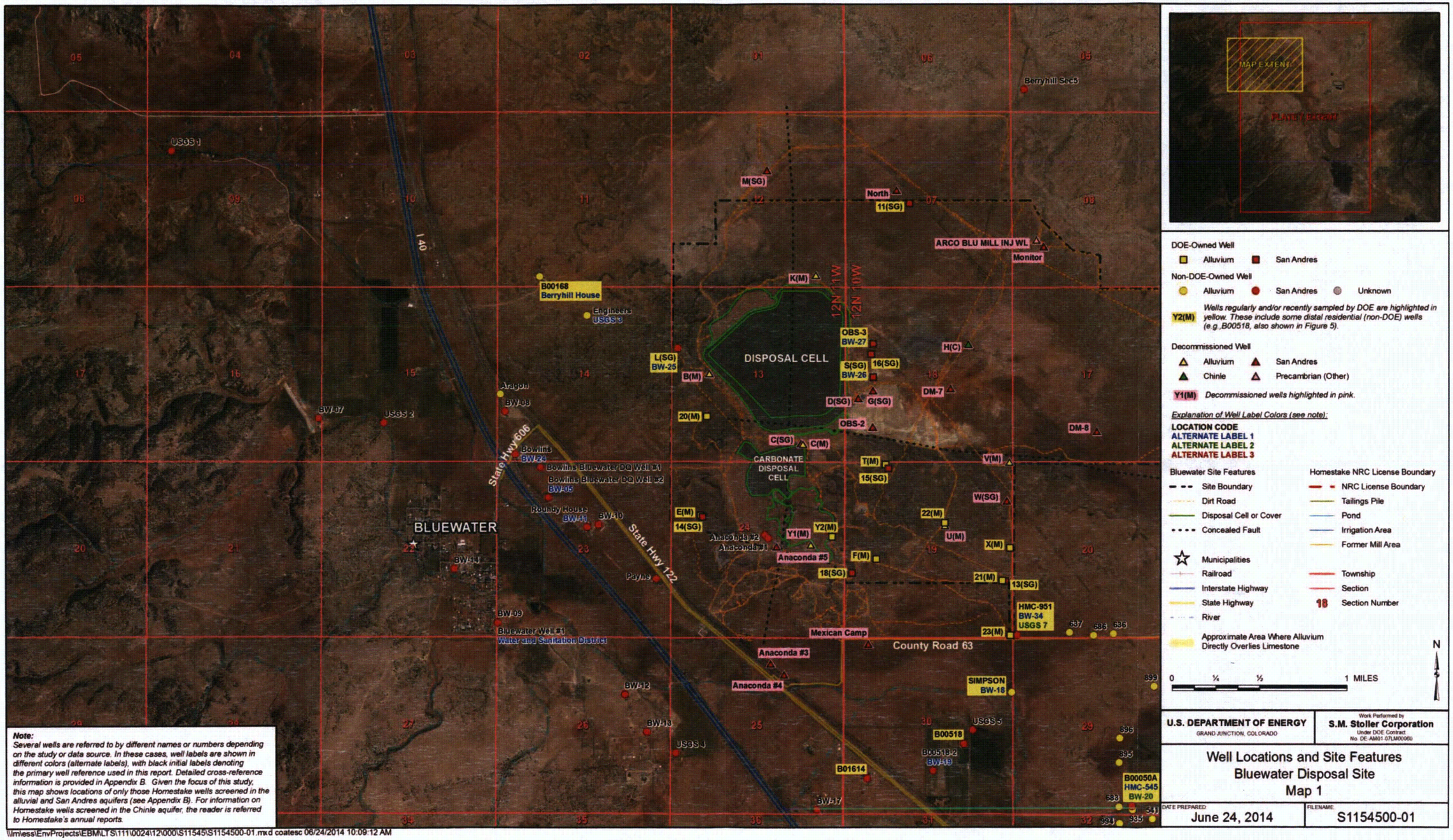

Figure 16. Monitoring Wells in the Study Area, Map 1 of 4

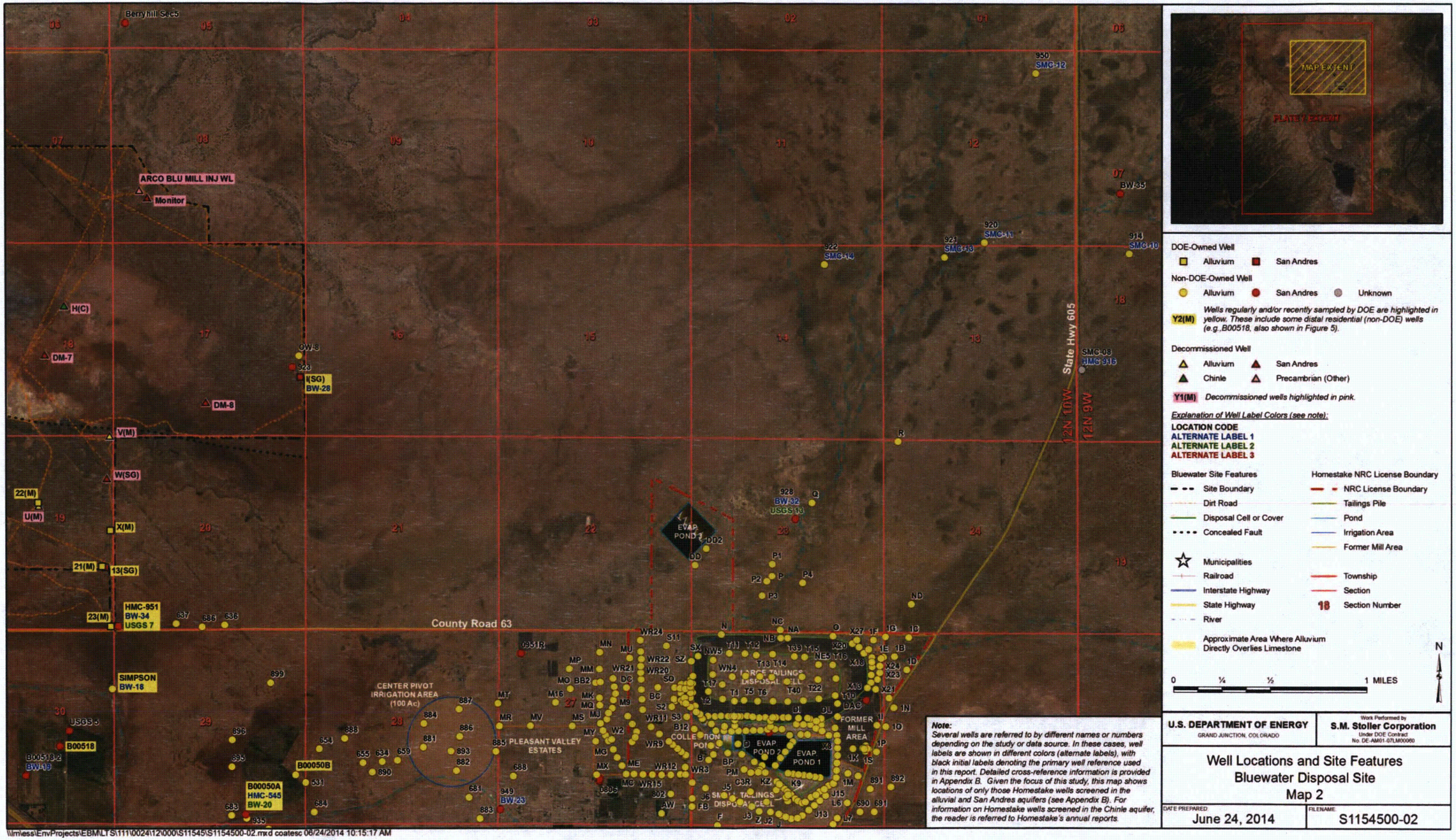

Figure 17. Monitoring Wells in the Study Area, Map 2 of 4

Figure 18. Monitoring Wells in the Study Area, Map 3 of 4

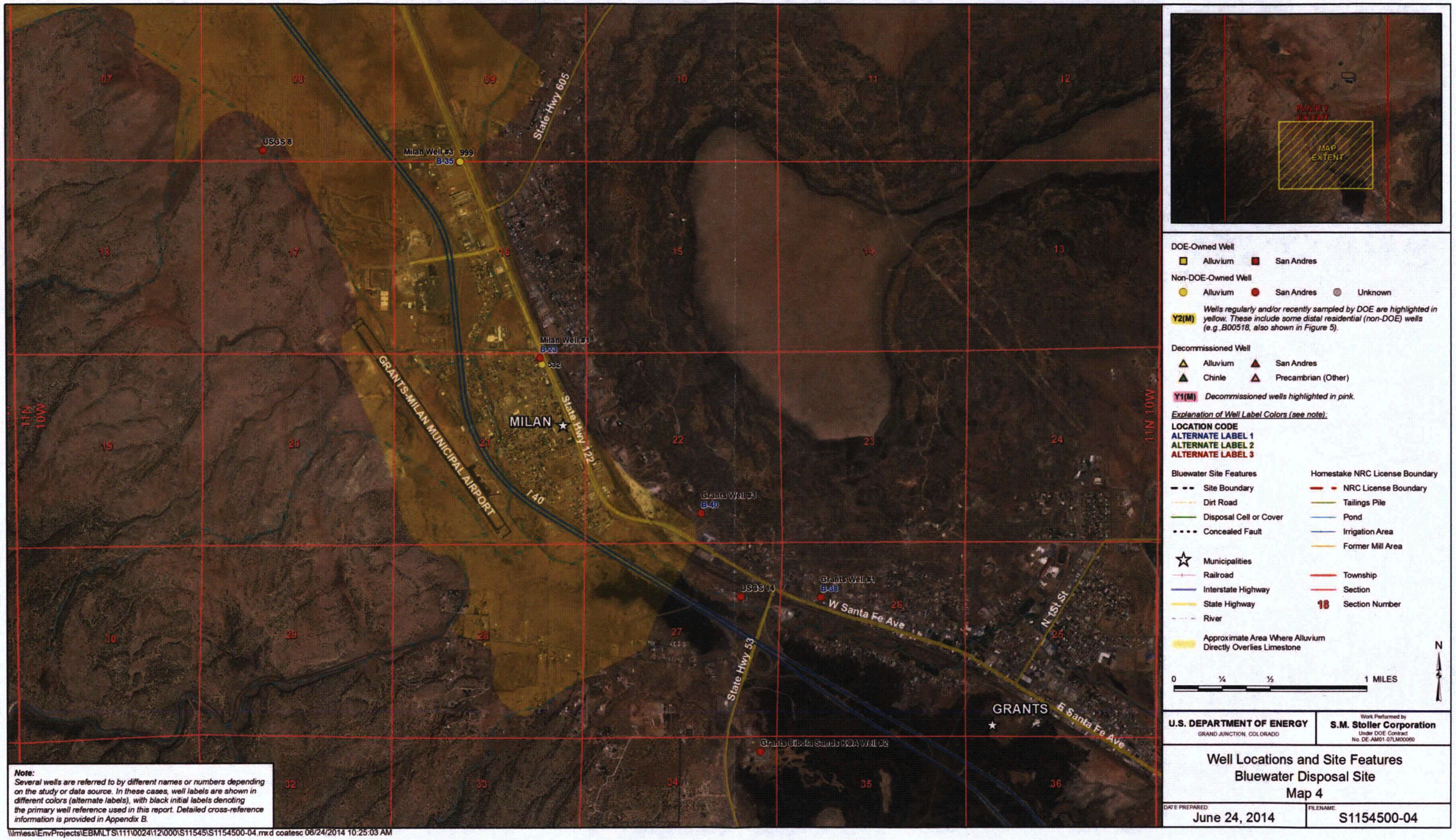

Figure 19. Monitoring Wells in the Study Area, Map 4 of 4

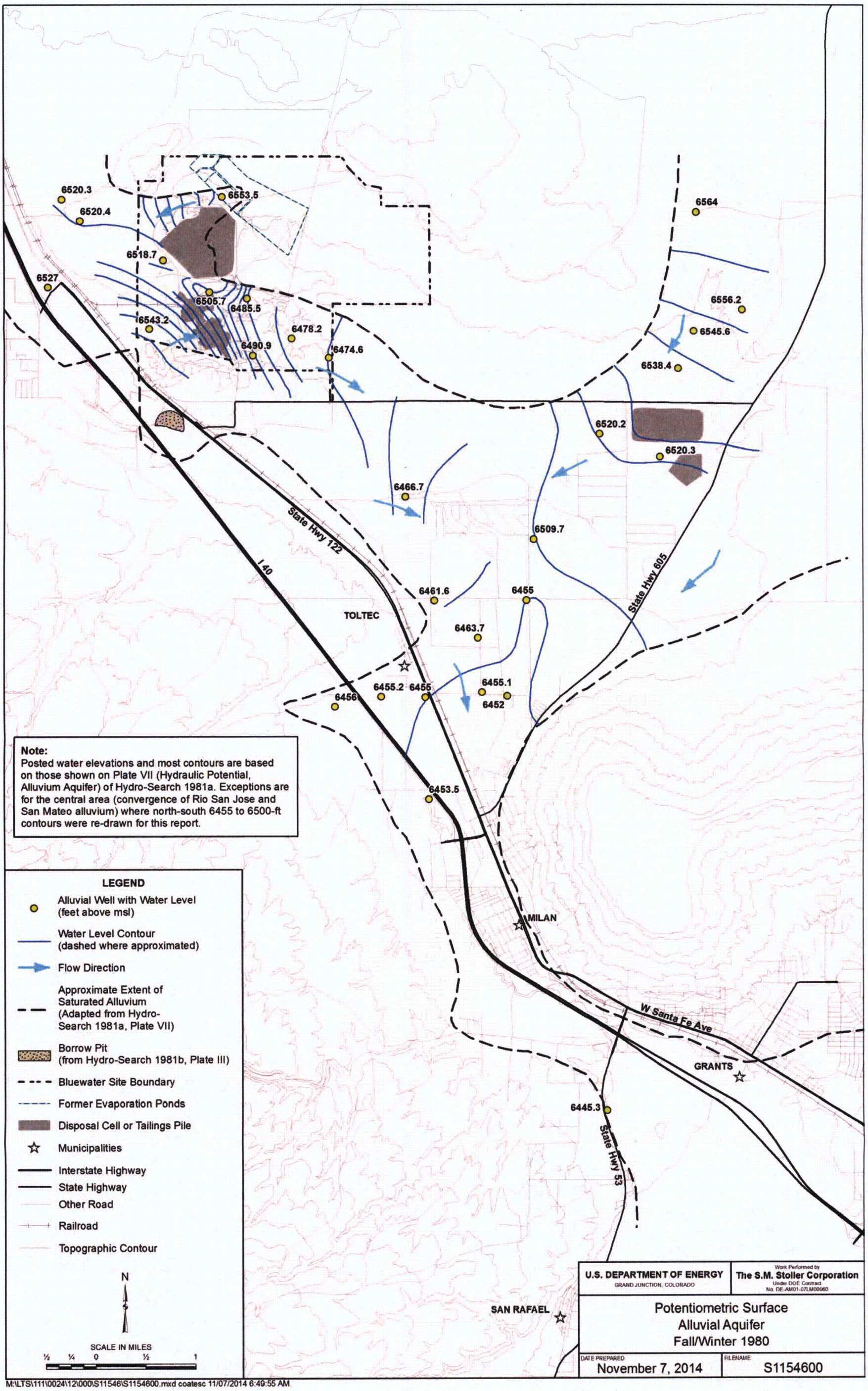

Figure 20. Hydraulic Heads in the Alluvial Aquifer in 1980

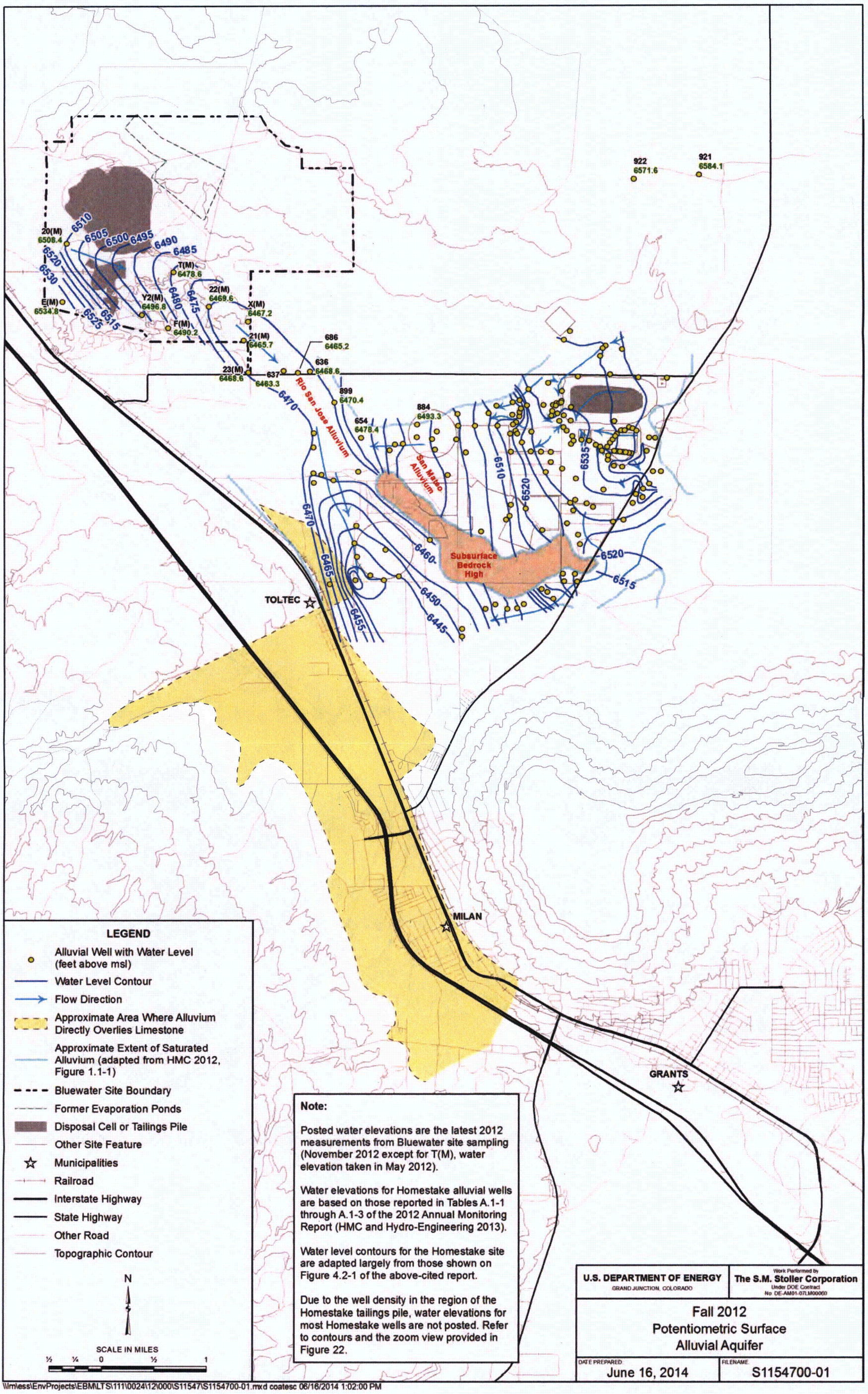

Figure 21. Hydraulic Heads in the Alluvial Aquifer in 2012

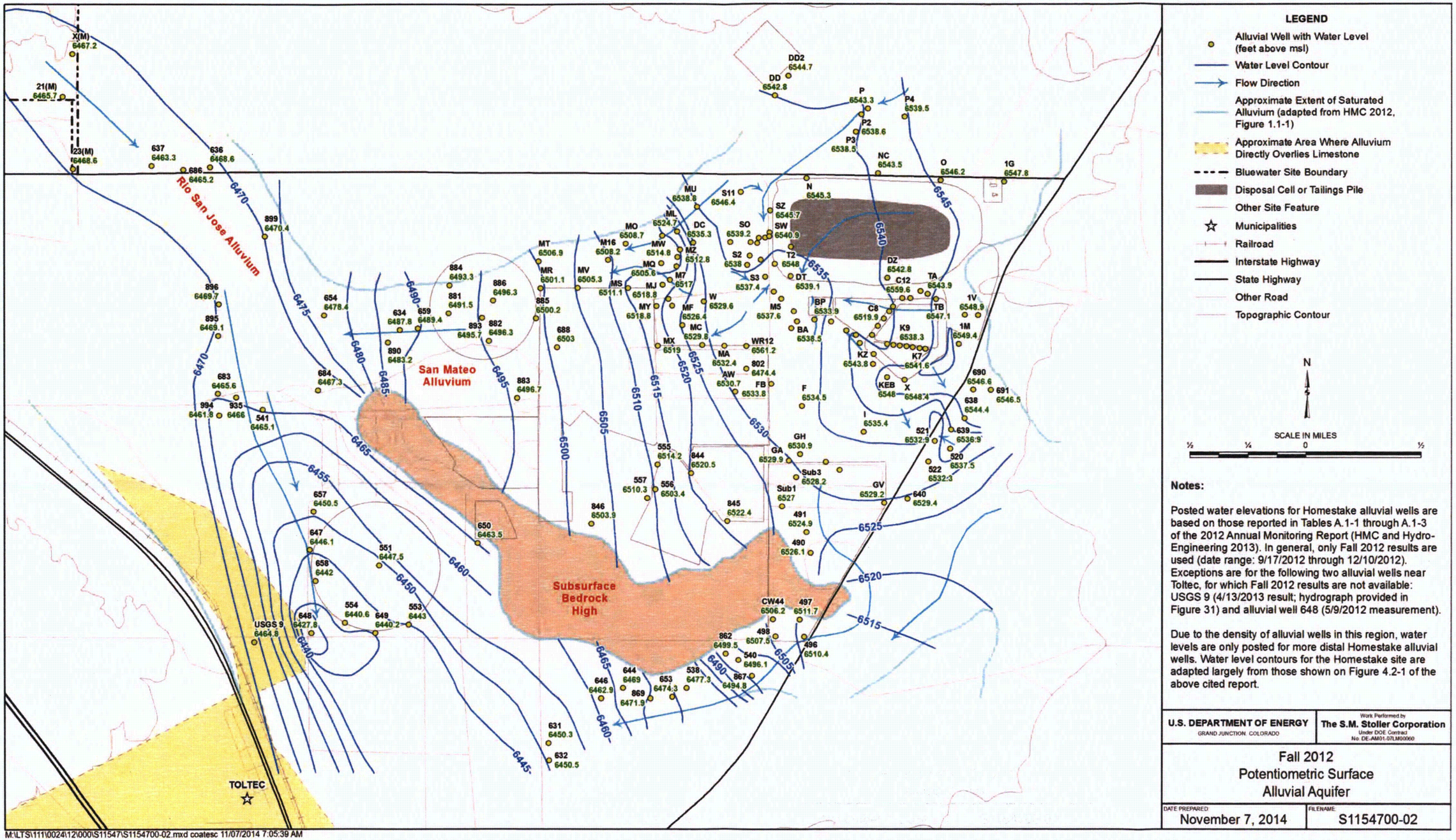

Figure 22. Hydraulic Heads and Flow Directions in the Alluvial Aquifer in 2012

This page intentionally left blank

As part of its investigation of regional hydrology features in the Grants-Bluewater Valley, Hydro-Search (1981a) also produced a map of the potentiometric surface in the San Andres aquifer as perceived in the late 1970s and early 1980s. Figure 23 presents a reproduction of that map. In general, the 1980 potentiometric surface in the San Andres aquifer showed groundwater migrating almost directly to the east in areas west of the main tailings impoundment and then heading in more of a southeast direction in areas east of the pile. This indicated that groundwater in the aquifer east of the Bluewater site was migrating in a direction transverse to the north-northeast dip of the San Andres Limestone and the Glorieta Sandstone. A particularly notable feature of the mapped surface in Figure 23 is the spatial variation in hydraulic gradients. The hydraulic gradient is relatively large in the area west of the main tailings impoundment, where estimates based on the mapped contours have values of 20 to 25 ft/mi, or 0.0038 to 0.0047 in dimensionless units. In contrast, the gradient flattens out considerably in areas east of the tailings impoundment, where estimated slopes of the potentiometric surface range from about 6.5 ft/mi (0.0012 dimensionless) immediately east of the impoundment to as little as 1 ft/mi (0.0002 dimensionless) in an area about 1.5 mi northwest of the large tailings disposal cell at the Homestake site. This general trend toward a flatter gradient east and southeast of the Bluewater site is a reflection of the large transmissivity zone between the Bluewater site and the San Rafael Fault (Section 4.2.4), which was assigned an average transmissivity of 50,000 ft^2/day by Baldwin and Anderholm (1992).

Comparison of the hydraulic heads in Figure 23 with measured groundwater levels in the alluvial aquifer in 1980 (Figure 20) indicates that heads in the ancestral river alluvium at the time were typically about 20 to 40 ft higher than those measured in the underlying bedrock aquifer. This meant that groundwater in the alluvium had the capacity to migrate downward to the San Andres aquifer where a hydraulic connection between the two aquifers occurs. For instance, downward migration of water from the alluvium to the San Andres in fault zones was a possibility, as was lateral movement of alluvial aquifer groundwater from south of the main tailings impoundment to the uplifted San Andres Limestone and Glorieta Sandstone just north of the East-West Fault.

Another notable feature of the potentiometric surface in Figure 23 was the difference in hydraulic heads between areas north and south of the East-West Fault at the Bluewater site. Heads north of the fault were generally about 5 to 10 ft higher than equivalent values south of the fault. Hydro-Search (1981a) identified this phenomenon as an indicator of the East-West Fault's capacity to act as a partial barrier to groundwater flow in the bedrock aquifer. Another notable feature of the potentiometric surface is the curvature of equipotentials south of the East-West Fault. Though a reason for this curvature was not given in the regional study of flow conditions (Hydro-Search 1981a), it was identified in an earlier assessment (Hydro-Search 1978) to represent the east and west edges of a pumping cone of influence centered in the area of the production wells Anaconda #1, Anaconda #3, and Anaconda #4. In the late 1970s and early 1980s, these wells were used to extract San Andres aquifer groundwater to support the milling activity.

Figure 24 presents a more recent depiction of the potentiometric surface in the San Andres aquifer. Because hydraulic head data were only available for a limited number of wells, the number of head contours used in this figure is considerably fewer than the number of contours used to illustrate the potentiometric surface in the aquifer in 1980 (Figure 23). Based on measured hydraulic heads in 2012, this surface shows that groundwater levels in the aquifer have, in more recent times, been considerably less than those observed in 1980. Despite the

obvious disparity in groundwater elevations between time periods, the general shape of the recent potentiometric surface and the groundwater flow direction implied by it are about the same as observed some 30 year earlier.

4.3.3.1 Flow Patterns in the San Andres Aquifer

Using hydraulic head data for the San Andres aquifer, Applied Hydrology Associates Inc. (1990) developed map views of general groundwater flow patterns in the aquifer. This conceptual model study built upon the earlier work to develop an updated map of flow directions in the aquifer (Figure 25). The flow vectors presented in this figure represent the flow paths taken by San Andres aquifer groundwater that originates beneath the Zuni Mountains in the vicinity of Bluewater Lake, and then migrates downgradient in eastward and east-southeastward directions, toward areas north of Milan and Grants. With a few minor exceptions, the flow directions shown in the updated figure are virtually identical to those identified by Applied Hydrology Associates Inc. (1990). Given that the flow directions in the San Andres aquifer appear to have changed little over the past 30 years, it is likely that the arcuate flow pattern pieced together from the vectors (Figure 25) has been present in the Grants-Bluewater Valley since the start of Bluewater mill operations in the 1950s.

Several features of the flow patterns map in Figure 25 have a bearing on contaminant transport. For example, groundwater flowing in the San Andres aquifer underneath the Bluewater site south of the East-West Fault appears to bypass the municipal wells for Milan, taking on a flow path that is about 1.5 to 2 mi north of the Milan public supply wells. Moreover, groundwater following this path appears to be heading for Grants as it passes under Black Mesa. Similarly, the flow path taken by water migrating beneath the Bluewater site north of the East-West Fault intersects the Homestake site both north and south of the large tailings disposal cell. Included in this wide flow path is groundwater that migrates east-southeastward from the northernmost boundary of the site, in the vicinity of the waste-injection well used between 1960 and 1977. The flow paths from Figure 25 imply that groundwater originating at the Bluewater site in areas north of the East-West Fault will pass beneath the Homestake site and continue flowing to the southeast to areas north of Grants.

The flow patterns map for the San Andres aquifer also indicates that recharge on the Zuni Mountains affects southeastward flow in the Grants-Bluewater Valley by pushing it farther to the north than would occur if this type of recharge were not present. This observation is important because it implies that recharge in the mountains is the primary reason that flow paths emanating from the Bluewater site pass well north of the Milan municipal wells.

4.3.3.2 Average Linear Velocities

The average linear velocity of groundwater in the alluvial and San Andres aquifers can be estimated using representative values of hydraulic conductivity, hydraulic gradient, and effective porosity for the two aquifers. Computed velocities based on estimates for these parameters in past investigations have varied widely. Similarly, estimated average linear velocities stemming from transport modeling studies of groundwater in different parts of the Grants-Bluewater Valley have covered a wide range. This report section attempts to develop general estimates of average linear velocity in the two aquifers, values that apply to the study area as a whole. Summaries of past studies and separate calculations based on Darcy's law are used to develop the estimates.

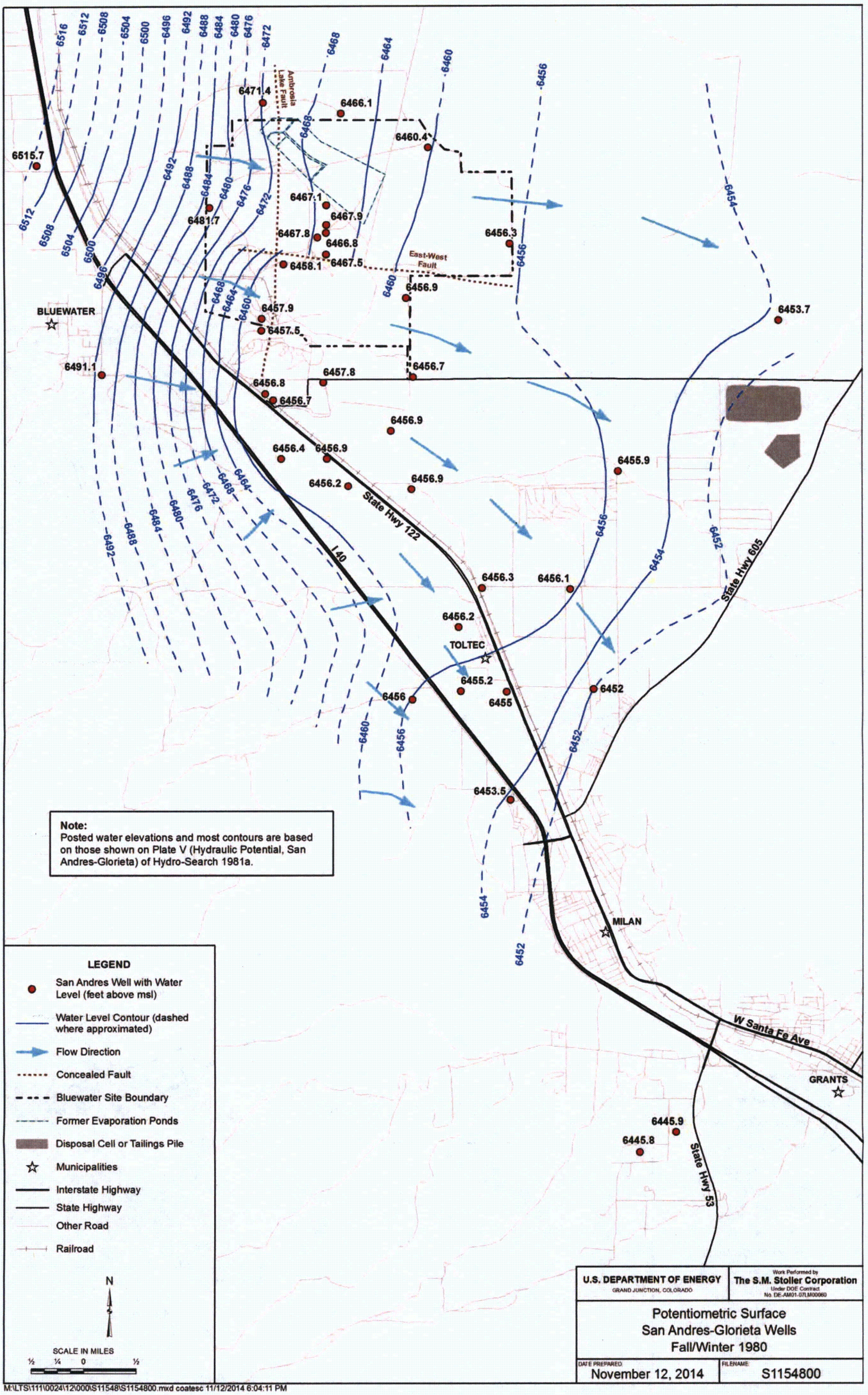

Figure 23. Potentiometric Surface in the San Andres Aquifer in 1980

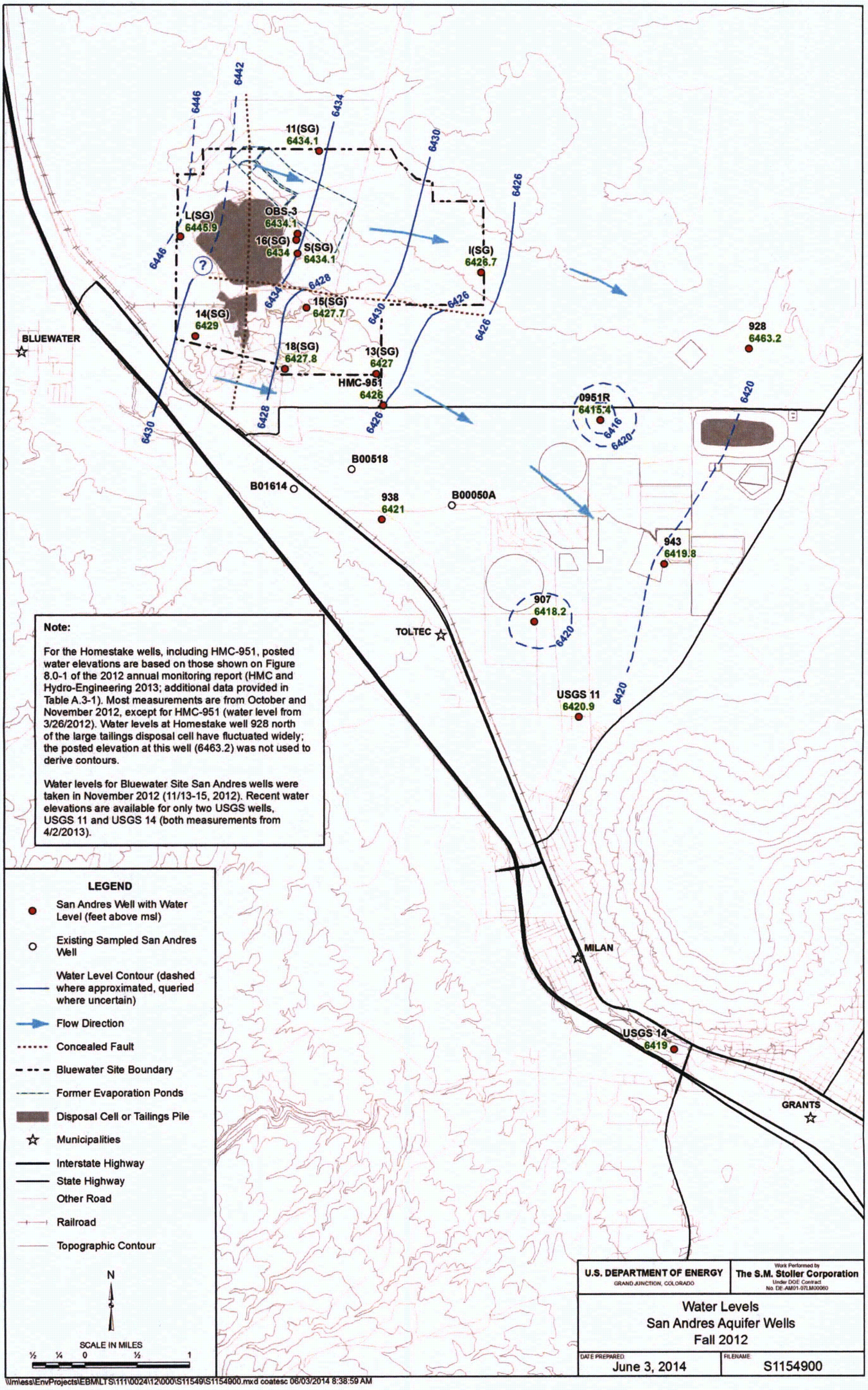

Figure 24. Potentiometric Surface in the San Andres Aquifer in 2012

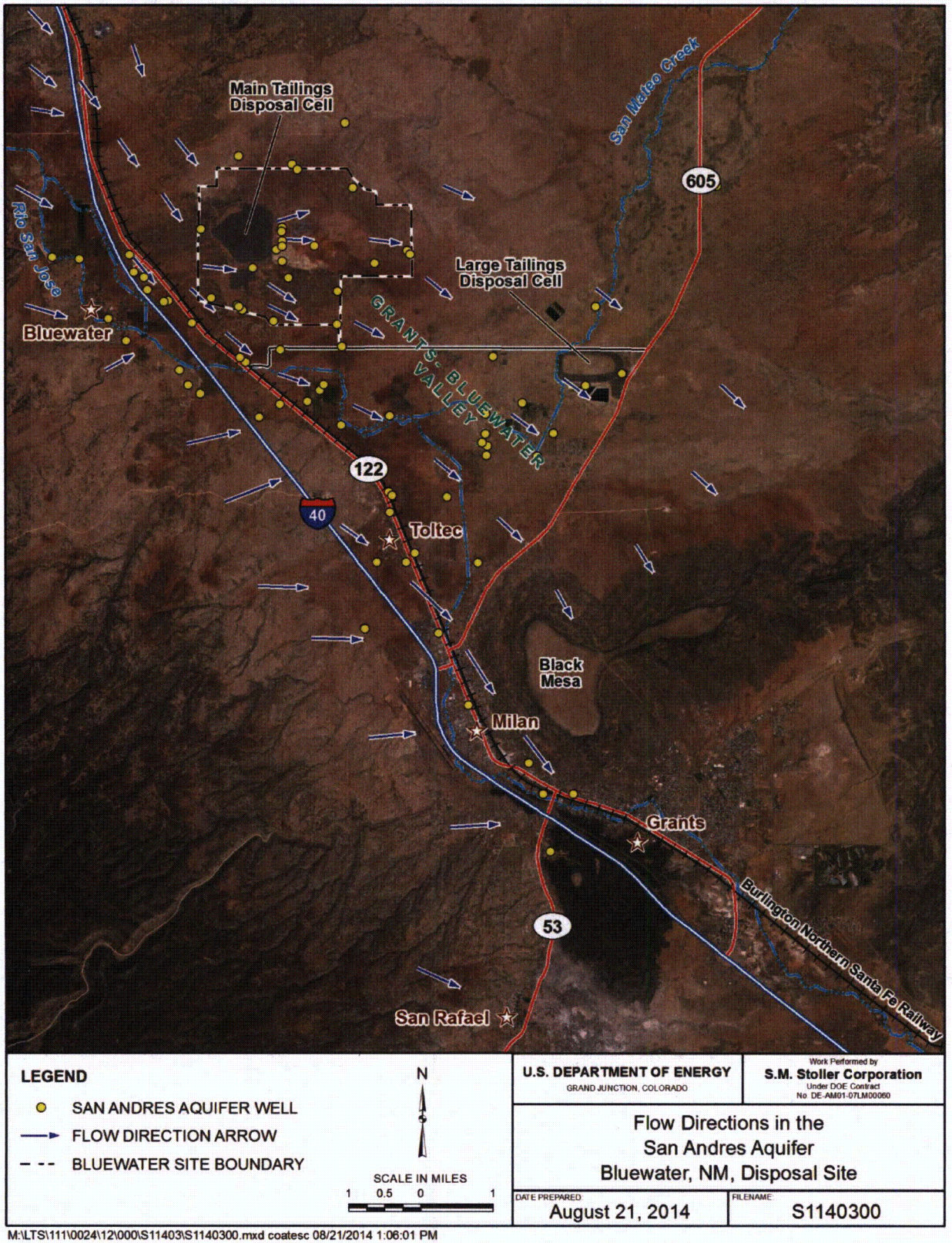

Figure 25. Ambient Flow Directions in the San Andres Aquifer

Hydro-Search (1977) estimated that the average linear velocity of groundwater flowing in ancestral river deposits within the alluvial aquifer at the Bluewater site could be as low as 300 feet per year (ft/yr [0.8 ft/day]) and as high as 1,000 ft/yr (2.75 ft/day). The corresponding estimated velocity for groundwater in the San Andres aquifer east of the main tailings impoundment was limited to 410 ft/yr (1.1 ft/day). All of the estimates by Hydro-Search (1977) were based on an assumed effective porosity of 0.25 in both the alluvial and San Andres aquifers.

In the course of calibrating transport models for groundwater in the Grants-Bluewater Valley, Dames & Moore (1986a) indicated that average linear velocity in the alluvial aquifer at the Bluewater site ranged from 4,500 to 9,000 ft/yr (12.3 to 24.6 ft/day). In the same study, the velocity of water migrating southeastward in the San Andres aquifer south of the East-West Fault at the Bluewater site was estimated to range from 1,800 to 6,000 ft/yr (4.9 to 16.4 ft/day). In comparison, Dames & Moore (1986a) estimated that groundwater flowing eastward in the San Andres aquifer from beneath the main tailings impoundment and north of the East-West Fault had a much slower velocity, varying from about 1,000 to 1,430 ft/yr (2.7 to 3.9 ft/day). The generally larger velocities estimated by Dames & Moore (1986a) for the San Andres aquifer in comparison to those estimated by Hydro-Search (1977) were attributed to the fact that the former assumed the effective porosity of the aquifer was 0.02. This much smaller porosity was used because it was considered more representative of flow in secondary permeability features in limestone, such as fractures, solution channels, and cavities.

Using the above-mentioned velocity estimates by others and information regarding the hydraulic parameters for the two aquifers (e.g., Sections 4.2.1 and 4.2.4), the conceptual model includes a preliminary summary of average linear velocities that could be expected in the various types of media composing the two aquifers (Table 3). In addition to showing a large range of velocities for the alluvial aquifer, the table also lists ranges for karst limestone media, the San Andres Limestone, and sandstone found in both the San Andres Limestone and the Glorieta Sandstone. The table listings suggest that very large velocities can be associated with conduit flow in karst features (fractures, solution channels, cavities) in the San Andres Limestone. Though the estimated velocities associated with unconsolidated sediments in the alluvial aquifer and sandstone media in the San Andres aquifer are smaller than those expected in karst media, the ranges attributed to alluvium and sandstone are similar in magnitude (Table 3).

Table 3. Estimated Ranges for Average Linear Velocity in Regional Aquifers Based on Previous Studies

Aquifer	Formation	Media Type	Flow Type	Average Linear Velocity Range	
				(ft/yr)	(ft/day)
Alluvial aquifer	Ancestral and Recent Rio San Jose alluvium, San Mateo Creek alluvium	alluvium (clay, silt, sand, gravel)	porous media	10–3,000	0.03–8.2
San Andres aquifer	San Andres Limestone	karst limestone (fractures, solution channels, cavities)	conduit	1,500–7,500	4.1–20.5
San Andres aquifer	San Andres Limestone and Glorieta Sandstone	unfractured and fractured sandstone	porous media and equivalent porous media[a]	250–1,500	0.7–4.1

[a] Equivalent porous media is a concept used to model or simulate the flow of groundwater in fractured rocks. The concept is that if the volume is large enough, the fractured geologic material will behave mathematically like a porous medium.

To further assess how groundwater flow in various types of subsurface media affects advective transport of contaminants, separate calculations of average linear velocity were prepared for parts of the two aquifers located downgradient (east and southeast) of the Bluewater site. The calculations were made using Equation 1.

$$v = q/n_e = KJ/n_e \quad (1)$$

where v = average linear velocity (length/time)
K = hydraulic conductivity (length/time)
J = horizontal hydraulic gradient (dimensionless)
n_e = effective porosity (dimensionless)

The computed velocities were subsequently used to estimate the times that would be required for a conservative (nonretarded) contaminant to migrate to specific locations downgradient of the Bluewater site. In the case of the alluvial aquifer, these estimates represented the time it would take for a contaminant to migrate from the south border of the main tailings disposal cell to a location near Toltec, and then on to Grants. In the case of the San Andres aquifer, travel times were calculated for a contaminant migrating from the east side of the main tailings disposal cell to the large tailings disposal cell at the Homestake site first, and then on to an area directly north of Grants. The travel times were calculated using Equation 2.

$$t_a = s_a/v \quad (2)$$

where t_a = travel time (days)
s_a = travel distance (ft)

One set of calculations based on equations 1 and 2 was made for the alluvial aquifer, whereas three different sets of computations were made to assess advection in the San Andres aquifer via (1) conduit flow in karst limestone, (2) equivalent porous media flow in fractured sandstone, and (3) porous media flow in unfractured sandstone. Multiple values of hydraulic conductivity and effective porosity considered representative of the various media in the aquifers were used in the calculations. Assumed hydraulic gradient values in the calculations were based on the potentiometric surface maps shown in Figure 20, Figure 21, Figure 23, and Figure 24.

The average linear-velocity and travel-time calculations for the alluvial aquifer, presented in Table 4, show a wide range in computed results. Of some interest is the fact that the minimum computed velocity for the alluvial aquifer is larger than the comparable minimum velocity shown in Table 3 for the alluvial aquifer, and the largest computed velocity in the alluvial aquifer is less than the comparable high end of the range listed in Table 3. The shortest travel time listed in Table 4 for the path between the south border of the main tailings disposal cell and a point immediately east of Toltec is 17 years (Velocity Calculation 4), which results from using a hydraulic conductivity of 180 ft/day and an effective porosity of 0.10. This result suggests that a contaminant such as uranium might have traveled as far as the Toltec area from the main tailings disposal cell as early as 1980, the first year of a comprehensive study of regional groundwater flow by Hydro-Search (1981a). In addition, the Table 4 calculations suggest that a conservative or mildly retarded contaminant could have reached the Toltec area well before the mid-1990s and easily by 2013, even if the effective porosity of the alluvial aquifer was as large as 0.25 (see Calculation 8).

It is less clear from the Table 4 calculations whether a conservative contaminant migrating in the alluvial aquifer from the main tailings disposal cell has presently traveled by advection as far downgradient as Grants. The shortest travel time for this route is 64 years (Velocity Calculation 12), which assumes a hydraulic conductivity of 180 ft/day and an effective porosity of 0.1. In comparison, about 60 years has passed between 1953, when milling at the Bluewater site started, and the year 2013. The comparable alluvial aquifer calculations based on an effective porosity of 0.25 (Calculations 13–16) suggest that at least 150 years would be required for the contamination originating at the main tailings disposal cell to migrate in the alluvial aquifer to as far as Grants (Table 4).

Table 5 shows the velocity and travel-time calculations for the San Andres aquifer. The calculations dealing with flow through secondary permeability features in the aquifer were based on the general observation that representative hydraulic conductivities for this type of flow tend to be high, and corresponding effective porosities are low (Worthington and Ford 2009). The range of hydraulic conductivities used to calculate travel times via conduits in karst limestone comported with the range of values compiled in Huntoon (1995) from tracer tests covering thousands to tens of thousands of feet of travel distance. Somewhat lower values of both hydraulic conductivity and effective porosity were used to represent equivalent porous medium flow in fractured sandstone.

As expected, the highest average linear velocities and shortest travel times are associated with conduit flow in karst limestone within the aquifer (Table 5), as these calculations are based on the very high hydraulic conductivities measured in solution-enlarged joints, solution channels, and cavities. Using hydraulic conductivities that range from 100 to 1,000 ft/day and effective porosities of 0.02 and 0.05, 7 of the 8 calculated travel times for the path between the east border of the main tailings disposal cell at the Bluewater site and the large tailings disposal cell at the Homestake site (4.5 miles) are 21 years or less (Table 5). This suggests a high probability that a conservative or mildly retarded contaminant migrating from the main tailings disposal cell solely through karst features reached the Homestake site by as early as 1980, when the regional hydrogeologic study by Hydro-Search (1981a) was initiated. The longest computed travel time via conduit flow between the two disposal cells, 57 years (Calculation 9), indicates that conservative contaminants would be present in the vicinity of the Homestake site today, if not as early as 1980. The computed average linear velocities for karst limestone features comport with the range of velocities reported by Huntoon (1995), which were derived from aquifer pumping tests in karst aquifers.

The eight calculations representing conduit flow from the main tailings disposal cell to an area directly north of Grants (Calculations 9 through 16 in Table 5) are of interest because six of the eight indicate that a nonretarded contaminant originating beneath the main tailings disposal cell in the mid- to late-1950s would have reached the area north of Grants before 2013. In general, the conduit-flow calculations suggest that mildly to nonretarded contamination originating in the San Andres aquifer at the Bluewater site in the 1950s probably reached the Homestake site by the early 1980s and has since migrated at least another 3 mi farther to the east and southeast.

Table 4. Average Linear Velocity Calculations for the Alluvial Aquifer

Calculation Number	From	To	Distance (s_a)		Estimated Gradient (J)	Hydraulic Conductivity (K)	Effective Porosity (n_e)	Average Linear Velocity (v)		Travel Time (t_a)
			(mi)	(ft)	(dimensionless)	(ft/day)	(dimensionless)	(ft/day)	(ft/yr)	(years)
1	South border of main tailings disposal cell	3500 ft directly east of Toltec	4.5	23,760	0.0021	20	0.1	0.42	154	155
2	South border of main tailings disposal cell	3500 ft directly east of Toltec	4.5	23,760	0.0021	60	0.1	1.26	461	52
3	South border of main tailings disposal cell	3500 ft directly east of Toltec	4.5	23,760	0.0021	120	0.1	2.53	922	26
4	South border of main tailings disposal cell	3500 ft directly east of Toltec	4.5	23,760	0.0021	180	0.1	3.79	1,383	17
5	South border of main tailings disposal cell	3500 ft directly east of Toltec	4.5	23,760	0.0021	20	0.25	0.17	61	387
6	South border of main tailings disposal cell	3500 ft directly east of Toltec	4.5	23,760	0.0021	60	0.25	0.51	184	129
7	South border of main tailings disposal cell	3500 ft directly east of Toltec	4.5	23,760	0.0021	120	0.25	1.01	369	64
8	South border of main tailings disposal cell	3500 ft directly east of Toltec	4.5	23,760	0.0021	180	0.25	1.52	553	43
9	South border of main tailings disposal cell	Grants	10	52,800	0.0013	20	0.1	0.25	92	573
10	South border of main tailings disposal cell	Grants	10	52,800	0.0013	60	0.1	0.76	277	191
11	South border of main tailings disposal cell	Grants	10	52,800	0.0013	120	0.1	1.52	553	95
12	South border of main tailings disposal cell	Grants	10	52,800	0.0013	180	0.1	2.27	830	64
13	South border of main tailings disposal cell	Grants	10	52,800	0.0013	20	0.25	0.10	37	1432
14	South border of main tailings disposal cell	Grants	10	52,800	0.0013	60	0.25	0.30	111	477
15	South border of main tailings disposal cell	Grants	10	52,800	0.0013	120	0.25	0.61	221	239
16	South border of main tailings disposal cell	Grants	10	52,800	0.0013	180	0.25	0.91	332	159

ft = feet; ft/day = feet per day; ft/yr = feet per year; mi = miles

Table 5. Average Linear Velocity Calculations for the San Andres Aquifer

Calculation Number	From	To	Flow Distance (s_a)		Estimated Gradient (J)	Hydraulic Conductivity (K)	Effective Porosity (n_e)	Average Linear Velocity (v)		Travel Time (t_a)
			(mi)	(ft)	(dimensionless)	(ft/day)	(dimensionless)	(ft/day)	(ft/yr)	(years)
Conduit Flow (fractures, solution channels and cavities in karst limestone)										
1	East Border of Main Tailings Disposal Cell	Homestake Large Tailings Cell	4.5	23,760	0.0006	100	0.02	3.16	1,152	21
2	East Border of Main Tailings Disposal Cell	Homestake Large Tailings Cell	4.5	23,760	0.0006	400	0.02	12.63	4,609	5
3	East Border of Main Tailings Disposal Cell	Homestake Large Tailings Cell	4.5	23,760	0.0006	700	0.02	22.10	8,065	3
4	East Border of Main Tailings Disposal Cell	Homestake Large Tailings Cell	4.5	23,760	0.0006	1000	0.02	31.57	11,521	2
5	East Border of Main Tailings Disposal Cell	Homestake Large Tailings Cell	4.5	23,760	0.0006	100	0.05	1.26	461	52
6	East Border of Main Tailings Disposal Cell	Homestake Large Tailings Cell	4.5	23,760	0.0006	400	0.05	5.05	1,843	13
7	East Border of Main Tailings Disposal Cell	Homestake Large Tailings Cell	4.5	23,760	0.0006	700	0.05	8.84	3,226	7
8	East Border of Main Tailings Disposal Cell	Homestake Large Tailings Cell	4.5	23,760	0.0006	1000	0.05	12.63	4,609	5
9	East Border of Main Tailings Disposal Cell	Directly north of Grants	7.5	39,600	0.0004	100	0.02	1.89	691	57
10	East Border of Main Tailings Disposal Cell	Directly north of Grants	7.5	39,600	0.0004	400	0.02	7.58	2,765	14
11	East Border of Main Tailings Disposal Cell	Directly north of Grants	7.5	39,600	0.0004	700	0.02	13.26	4,839	8
12	East Border of Main Tailings Disposal Cell	Directly north of Grants	7.5	39,600	0.0004	1000	0.02	18.94	6,913	6
13	East Border of Main Tailings Disposal Cell	Directly north of Grants	7.5	39,600	0.0004	100	0.05	0.76	277	143
14	East Border of Main Tailings Disposal Cell	Directly north of Grants	7.5	39,600	0.0004	400	0.05	3.03	1,106	36
15	East Border of Main Tailings Disposal Cell	Directly north of Grants	7.5	39,600	0.0004	700	0.05	5.30	1,936	20
16	East Border of Main Tailings Disposal Cell	Directly north of Grants	7.5	39,600	0.0004	1000	0.05	7.58	2,765	14

Table 5 (continued). Average Linear Velocity Calculations for the San Andres Aquifer

Calculation Number	From	To	Flow Distance (s_a)		Estimated Gradient (J)	Hydraulic Conductivity (K)	Effective Porosity (n_e)	Average Linear Velocity (v)		Travel Time (t_a)
			(mi)	(ft)	(dimensionless)	(ft/day)	(dimensionless)	(ft/day)	(ft/yr)	(years)
Fracture Flow in Sandstone (equivalent porous media)										
17	East Border of Main Tailings Disposal Cell	Homestake Large Tailings Cell	4.5	23,760	0.0006	20	0.01	1.26	461	52
18	East Border of Main Tailings Disposal Cell	Homestake Large Tailings Cell	4.5	23,760	0.0006	50	0.01	3.16	1,152	21
19	East Border of Main Tailings Disposal Cell	Homestake Large Tailings Cell	4.5	23,760	0.0006	100	0.01	6.31	2,304	10
20	East Border of Main Tailings Disposal Cell	Homestake Large Tailings Cell	4.5	23,760	0.0006	150	0.01	9.47	3,456	7
21	East Border of Main Tailings Disposal Cell	Homestake Large Tailings Cell	4.5	23,760	0.0006	20	0.02	0.63	230	103
22	East Border of Main Tailings Disposal Cell	Homestake Large Tailings Cell	4.5	23,760	0.0006	50	0.02	1.58	576	41
23	East Border of Main Tailings Disposal Cell	Homestake Large Tailings Cell	4.5	23,760	0.0006	100	0.02	3.16	1,152	21
24	East Border of Main Tailings Disposal Cell	Homestake Large Tailings Cell	4.5	23,760	0.0006	150	0.02	4.73	1,728	14
25	East Border of Main Tailings Disposal Cell	Directly north of Grants	7.5	39,600	0.0004	20	0.01	0.76	277	143
26	East Border of Main Tailings Disposal Cell	Directly north of Grants	7.5	39,600	0.0004	50	0.01	1.89	691	57
27	East Border of Main Tailings Disposal Cell	Directly north of Grants	7.5	39,600	0.0004	100	0.01	3.79	1,383	29
28	East Border of Main Tailings Disposal Cell	Directly north of Grants	7.5	39,600	0.0004	150	0.01	5.68	2,074	19
29	East Border of Main Tailings Disposal Cell	Directly north of Grants	7.5	39,600	0.0004	20	0.02	0.38	138	286
30	East Border of Main Tailings Disposal Cell	Directly north of Grants	7.5	39,600	0.0004	50	0.02	0.95	346	115
31	East Border of Main Tailings Disposal Cell	Directly north of Grants	7.5	39,600	0.0004	100	0.02	1.89	691	57
32	East Border of Main Tailings Disposal Cell	Directly north of Grants	7.5	39,600	0.0004	150	0.02	2.84	1,037	38

Table 5 (continued). Average Linear Velocity Calculations for the San Andres Aquifer

Calculation Number	From	To	Flow Distance (s_a)		Estimated Gradient (J)	Hydraulic Conductivity (K)	Effective Porosity (n_e)	Average Linear Velocity (v)		Travel Time (t_a)
			(mi)	(ft)	(dimensionless)	(ft/day)	(dimensionless)	(ft/day)	(ft/yr)	(years)
Sandstone (porous media flow)										
33	East Border of Main Tailings Disposal Cell	Homestake Large Tailings Cell	4.5	23,760	0.0006	0.1	0.075	0.001	0.3	85,927
34	East Border of Main Tailings Disposal Cell	Homestake Large Tailings Cell	4.5	23,760	0.0006	1	0.075	0.01	3	8,593
35	East Border of Main Tailings Disposal Cell	Homestake Large Tailings Cell	4.5	23,760	0.0006	5	0.075	0.04	14	1,719
36	East Border of Main Tailings Disposal Cell	Homestake Large Tailings Cell	4.5	23,760	0.0006	20	0.075	0.15	55	430
37	East Border of Main Tailings Disposal Cell	Homestake Large Tailings Cell	4.5	23,760	0.0006	0.1	0.125	0.0005	0.2	143,211
38	East Border of Main Tailings Disposal Cell	Homestake Large Tailings Cell	4.5	23,760	0.0006	1	0.125	0.005	2	14,321
39	East Border of Main Tailings Disposal Cell	Homestake Large Tailings Cell	4.5	23,760	0.0006	5	0.125	0.02	8	2,864
40	East Border of Main Tailings Disposal Cell	Homestake Large Tailings Cell	4.5	23,760	0.0006	20	0.125	0.09	33	716
41	East Border of Main Tailings Disposal Cell	Directly north of Grants	7.5	39,600	0.0005	0.1	0.075	0.001	0.2	214,816
42	East Border of Main Tailings Disposal Cell	Directly north of Grants	7.5	39,600	0.0005	1	0.075	0.01	2	21,482
43	East Border of Main Tailings Disposal Cell	Directly north of Grants	7.5	39,600	0.0005	5	0.075	0.03	11	4,296
44	East Border of Main Tailings Disposal Cell	Directly north of Grants	7.5	39,600	0.0005	20	0.075	0.12	44	1,074
45	East Border of Main Tailings Disposal Cell	Directly north of Grants	7.5	39,600	0.0005	0.1	0.125	0.0004	0.1	358,027
46	East Border of Main Tailings Disposal Cell	Directly north of Grants	7.5	39,600	0.0005	1	0.125	0.004	1	35,803
47	East Border of Main Tailings Disposal Cell	Directly north of Grants	7.5	39,600	0.0005	5	0.125	0.02	7	7,161
48	East Border of Main Tailings Disposal Cell	Directly north of Grants	7.5	39,600	0.0005	20	0.125	0.07	27	1,790

ft = feet; ft/day = feet per day; ft/yr = feet per year; mi = miles

The average linear velocity calculations representing equivalent porous media flow in fractured sandstone in the San Andres aquifer (Calculations 17 through 32 in Table 5) were based on estimated hydraulic conductivities that were smaller than those used to represent conduit flow and effective porosities that were equal to or smaller than those assigned to karst conduits. The two effective porosities adopted for these calculations, 0.01 and 0.02, were based on the assumption that the percentage of bulk cross-sectional area of sandstone represented by fractures was very small. Under these assumptions, the resulting calculations suggest that average linear velocities in fractured sandstone are not much smaller than those for conduit flow, and, accordingly, travel times are not much longer. In fact, 5 of the 8 calculated travel times for the 4.5 mi between the main tailings disposal cell and the large tailings disposal cell at the Homestake site are 21 years or less, suggesting that mildly to nonretarded contaminants originating at the Bluewater site reached the Homestake site by 1980. In addition, 7 of the 8 calculations for this path show travel times of 52 years or less, suggesting that conservative contaminants arrived at the Homestake site at least during recent years, if not by as early as 1980. With one exception (Calculation 28), the computed travel times for fractured sandstone flow between the main tailings disposal cell and the area directly north of Grants indicate that contaminants did not migrate the full 7.5 mi distance as of 1980. However, three of the eight calculations for this path suggest that conservative contaminants did cover the full distance by 2013.

Computed travel times for advective transport in fractured sandstone of the San Andres aquifer (Calculations 17 through 32) indicate that this type of transport is close to being as effective as conduit flow in quickly delivering conservative or mildly retarded contamination from the Bluewater site to downgradient locations. However, it is difficult to conceptualize that fracture systems in sandstone within the aquifer are connected over the full 4.5 mi distance between the main tailings disposal cell and the large tailings disposal cell at the Homestake site. Rather, it seems more likely that some combination of conduit flow in limestone and fracture flow in sandstone could facilitate rapid transport of conservative constituents in groundwater between the two sites. Regardless of the specific forms of groundwater flow that govern advection of contaminants between the two sites, the presence of secondary permeability features (fractures, solutions channels, cavities) in the San Andres aquifer enhances the potential for rapid contaminant transport. Given the large span of computed travel times between the two sites under conduit and fractured-sandstone flow (Calculations 1 through 32 in Table 5), influxes of Bluewater-derived contamination at downgradient locations over several decades appears possible.

In contrast to the conduit flow and fractured sandstone assessments, the calculations considered representative of porous media flow in unfractured sandstone (Calculations 33 through 48 in Table 5) suggest that average linear velocities in this type of medium are very low, ranging from 0.3 to 55 ft/yr. This is mostly attributed to the relatively small hydraulic conductivities (0.1 to 20 ft/day) adopted in the calculations for this type of transport, which were based on the assumption that calcareous and silica cements in sandstone pores greatly limit the rock's permeability. Cementation of sandstone pores was also used to justify relatively small effective porosities (0.075 and 0.125) in the porous media calculations (in comparison to porosities of 0.2 to 0.35 in unconsolidated sands). The computed velocities for unfractured sandstone remained very low, and the calculated travel times were on the order of hundreds of years (Table 5). These results strongly suggest that contamination migrating from the Bluewater site in unfractured sandstone is unlikely to ever reach the Homestake site via horizontal transport.

Instead, the non-fractured sandstone is expected to function more like a rock matrix in a fracture-matrix system, with contamination exchanging between the matrix and secondary porosity features such as fractures, solution channels, and cavities via molecular diffusion and very slow advection.

The calculations summarized in Table 4 and Table 5 indicate that estimates of average linear velocity discussed in earlier studies (e.g., Hydro-Search 1977, Dames & Moore 1986a) are reflective of water movement in the most permeable media within each aquifer. This is not surprising given that groundwater flow velocities are often estimated on the basis of first arrival of contaminants at locations downgradient of contaminant sources. However, the presence of lower-permeability sediments in both aquifers (silts and clays in alluvium, unfractured sandstone in the San Andres aquifer) suggests that contamination residing within them will be slowly released to more permeable pathways through diffusion processes (back diffusion), causing contaminants to persist in groundwater much longer (e.g., Chapman et al. 2012) than if transport was limited to high-permeability media. With respect to uranium transport in groundwater, the slow back diffusion would cause long-term "tailing" of uranium concentrations at downgradient locations, even if contaminant sources at the Bluewater site were eventually removed.

4.3.4 Influence of Faults

Faults in the San Andres aquifer affect groundwater flow, partly by blocking flow where vertical offset of the aquifer occurs. Changes in the gradient of the regional potentiometric surface may result from the blockages, such that changes in hydraulic head upgradient and downgradient of fault zones are small, and significant drops in hydraulic heads are observed within the relatively short width of each fault zone (e.g., Frenzel 1992). Faults could also affect the flow of groundwater by providing a preferential flow path for vertical seepage (e.g., Bense and Person 2006).

Faults in the study area can also influence subsurface flow by creating anisotropy in local hydraulic conductivity (variations in hydraulic conductivity with direction of measurement) of the San Andres aquifer. In areas where the amount of offset of faults is slight, hydraulic conductivity in a particular direction may be enhanced by development of solution channels along the fault in the San Andres Limestone and by fracturing in the Glorieta Sandstone. Joint sets in the aquifer framework also may result in anisotropy of hydraulic conductivity.

North- to northeast-trending faults or fault zones have the capacity to block the regional flow of water in the San Andres aquifer within the study area. The impacts vary from mild to significant depending on the magnitude of offset of the aquifer provided by the fault. The south end of Big Draw Fault impacts groundwater flow near the mouth of Bluewater Canyon. However, the offset of the fault is less than the thickness of the San Andres aquifer, and groundwater flow does not appear to be severely blocked by the fault.

The Ambrosia Lake Fault, which traverses the Bluewater site in a north-south direction, appears to act as a partial barrier to eastward-flowing groundwater in the San Andres aquifer. Local offset at the fault in the vicinity of the main tailings impoundment is at least 300 ft. Inspection of hydraulic head data collected from San Andres aquifer wells at the site over the past 3 years suggests that the drop in head across the fault in areas north of the East-West Fault is about 8 ft. In areas south of the East-West Fault, hydraulic head drops across the Ambrosia Lake Fault appear to be minimal to nonexistent due to insignificant displacement along the fault in that area.

The San Rafael Fault near Grants blocks west-to-east flow from Ojo del Gallo northeastward to a point near the Cibola-McKinley county line. Southwest from Ojo del Gallo, the offset of the San Rafael Fault may not exceed the thickness of the San Andres aquifer. At Ojo del Gallo, the San Rafael Fault forces the water table to rise above the land surface, causing the spring. The head difference across the fault, estimated at about 30 ft in Frenzel (1992), indicates that the fault is a major barrier to groundwater flow.

4.3.5 Regional Hydrographs

Regional groundwater levels have changed significantly over the past 65 years, depending on varying annual precipitation quantities and groundwater withdrawals from wells in the Grants-Bluewater Valley. The magnitude and duration of those changes can be seen by examining hydrographs from USGS monitoring wells in the study area.

Figure 26 is a map showing the locations of 14 USGS wells in the region and the geologic units that the wells are screened in. Hydrographs for the wells are presented here to illustrate the duration and magnitude of the changes observed in sub-areas of Grants-Bluewater Valley. The hydrographs show measured water levels in San Andres aquifer wells dating back to as early as the mid-1940s.

Figure 27 presents historical hydrographs for two wells screened in the San Andres aquifer in an area that represents groundwater-level changes in the vicinity of the Bluewater site and Bluewater Village (Bluewater Area). Figure 28 contains hydrographs for four wells located farther to the south, southeast of the Bluewater site (Mid-Valley Area), and Figure 29 shows hydrographs for four wells near the south end of the Grants-Bluewater Valley (South Valley Area). Hydraulic head changes since 1946 in each of these groups of wells illustrate that the San Andres aquifer has experienced regional head variations on the order of 70 ft or more. Some of the more notable changes were observed from the mid-1940s through the late 1950s, a period during which pumping for agricultural irrigation increased greatly. Some of the regional head declines in the late 1950s were also attributed to groundwater withdrawals for uranium-milling purposes. From the early 1960s until the early 1980s, measured water elevations in San Andres aquifer wells fluctuated but did not show any major increases or declines. Water elevations in most San Andres aquifer wells then increased steadily until the late 1980s (Figure 27 through Figure 29), and in some wells achieved water levels that exceeded those initially observed in the mid-1940s. As shown in Figure 28 and Figure 29, hydraulic heads in the bedrock aquifer have declined substantially since the late 1990s, in some cases as much as 50 to 60 ft.

Two additional hydrographs are illustrated in Figure 30 for wells screened in the San Andres aquifer in the vicinity of the Homestake site. Though trends in hydraulic head at one of these locations (USGS 13 [HMC-928]) prior to the early 1980s were similar to those discussed earlier for wells in the Bluewater, Mid-Valley, and South Valley Areas, anomalous changes have been observed at this location (north of the large tailings disposal cell) since the early 2000s. Specifically, heads have increased at this well during the past 10 years (2004–2013) instead of declining as observed at other San Andres aquifer wells during the same period. Though the reason for this increase is unknown, EPA (2011) has speculated that the groundwater remedy at the GRP creates conditions that promote downward leakage of alluvial aquifer groundwater across the Chinle Formation within branches of the San Mateo Fault, thus increasing hydraulic head in the underlying San Andres aquifer.

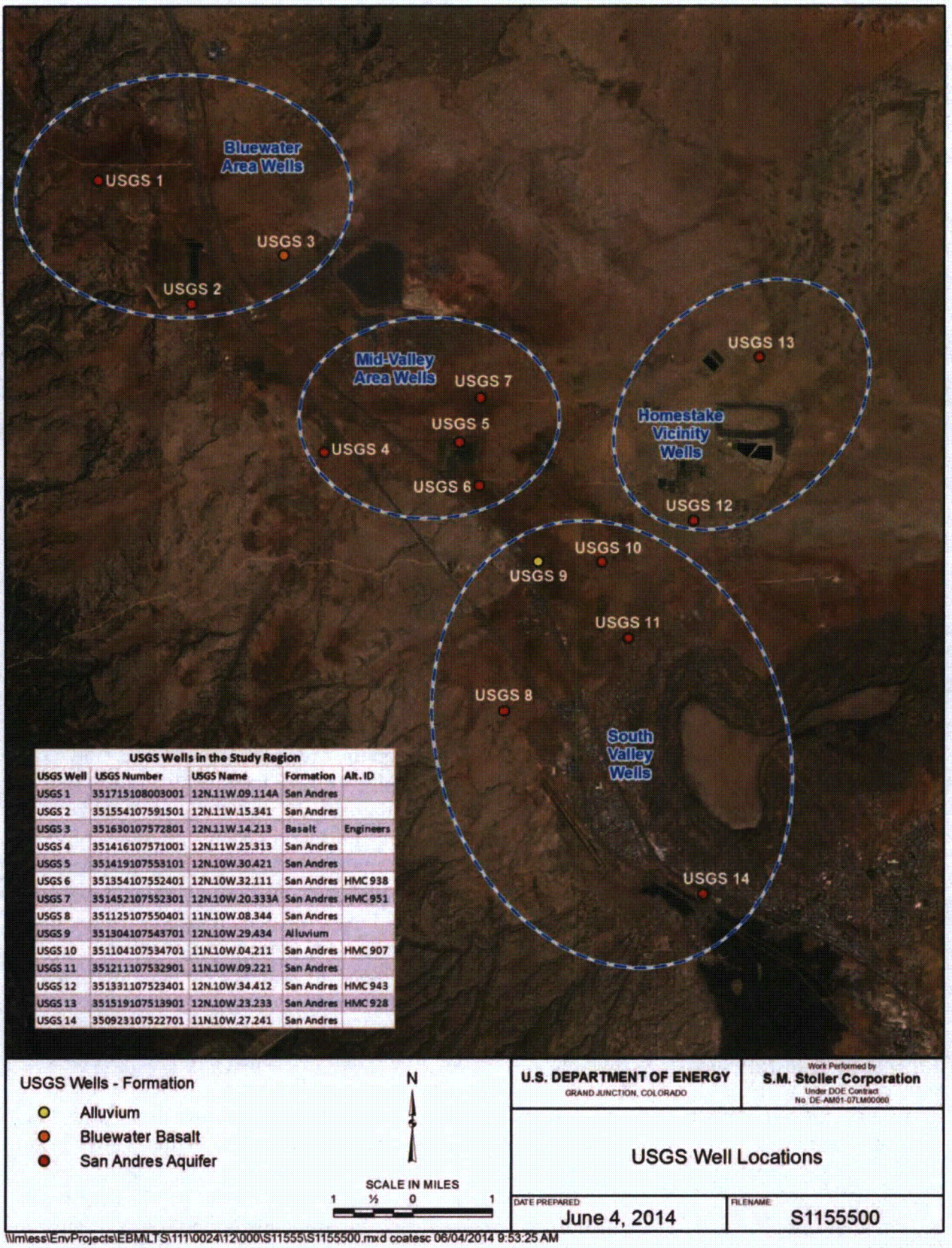

USGS Wells in the Study Region

USGS Well	USGS Number	USGS Name	Formation	Alt. ID
USGS 1	351715108003001	12N.11W.09.114A	San Andres	
USGS 2	351554107591501	12N.11W.15.341	San Andres	
USGS 3	351630107572801	12N.11W.14.213	Basalt	Engineers
USGS 4	351416107571001	12N.11W.25.313	San Andres	
USGS 5	351419107553101	12N.10W.30.421	San Andres	
USGS 6	351354107552401	12N.10W.32.111	San Andres	HMC 938
USGS 7	351452107552301	12N.10W.20.333A	San Andres	HMC 951
USGS 8	351125107550401	11N.10W.08.344	San Andres	
USGS 9	351304107543701	12N.10W.29.434	Alluvium	
USGS 10	351104107534701	11N.10W.04.211	San Andres	HMC 907
USGS 11	351211107532901	11N.10W.09.221	San Andres	
USGS 12	351331107523401	12N.10W.34.412	San Andres	HMC 943
USGS 13	351519107513901	12N.10W.23.233	San Andres	HMC 928
USGS 14	350923107522701	11N.10W.27.241	San Andres	

Figure 26. USGS Monitoring Wells in the Study Area

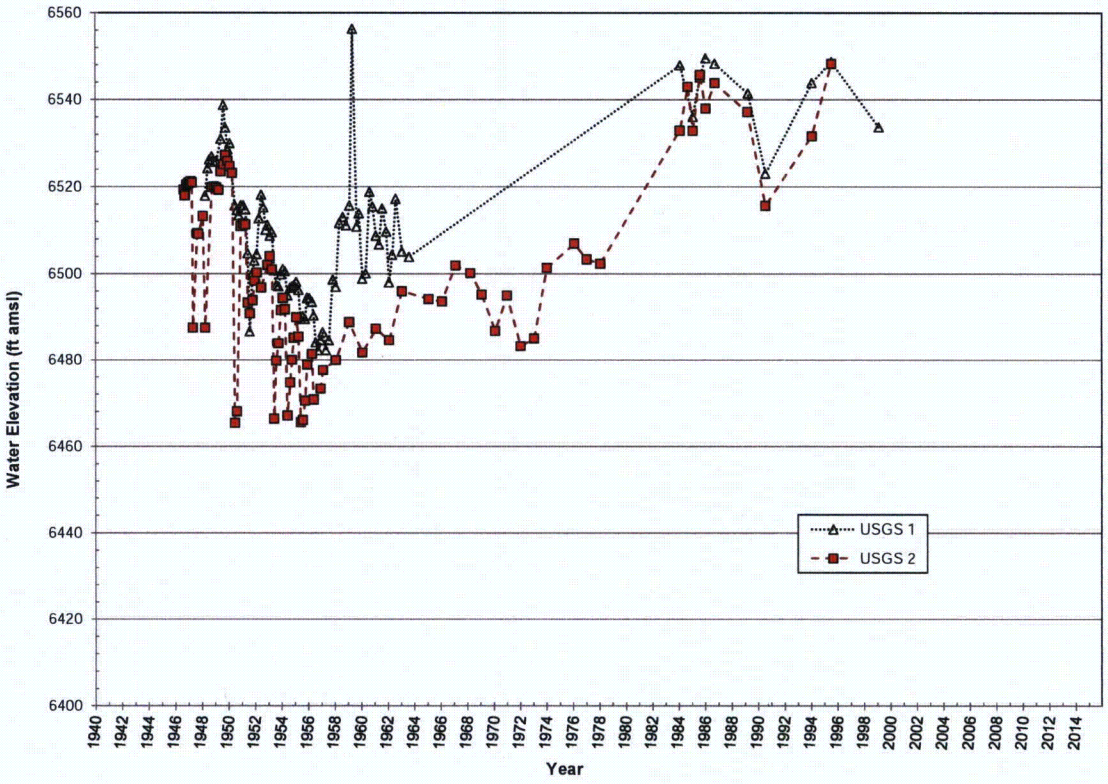

Figure 27. Hydrographs for USGS Wells Screened in the San Andres Aquifer in the Bluewater Area

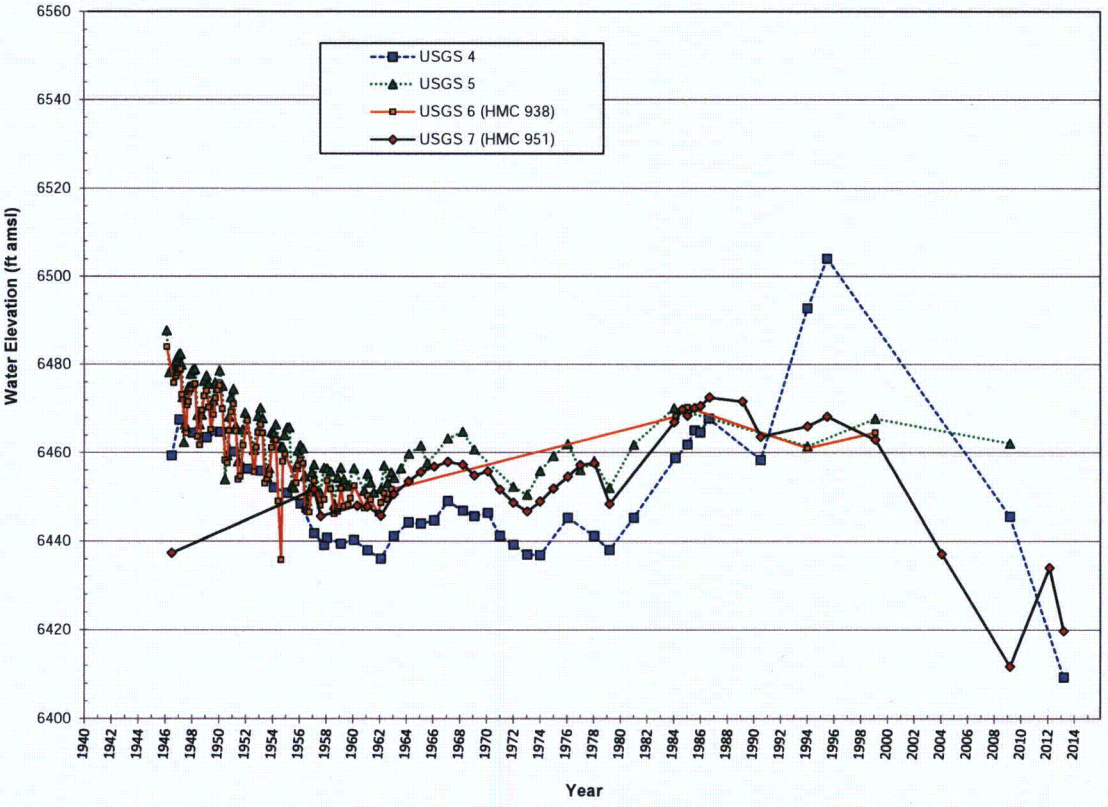

Figure 28. Hydrographs for USGS Wells Screened in the San Andres Aquifer in the Mid-Valley Area

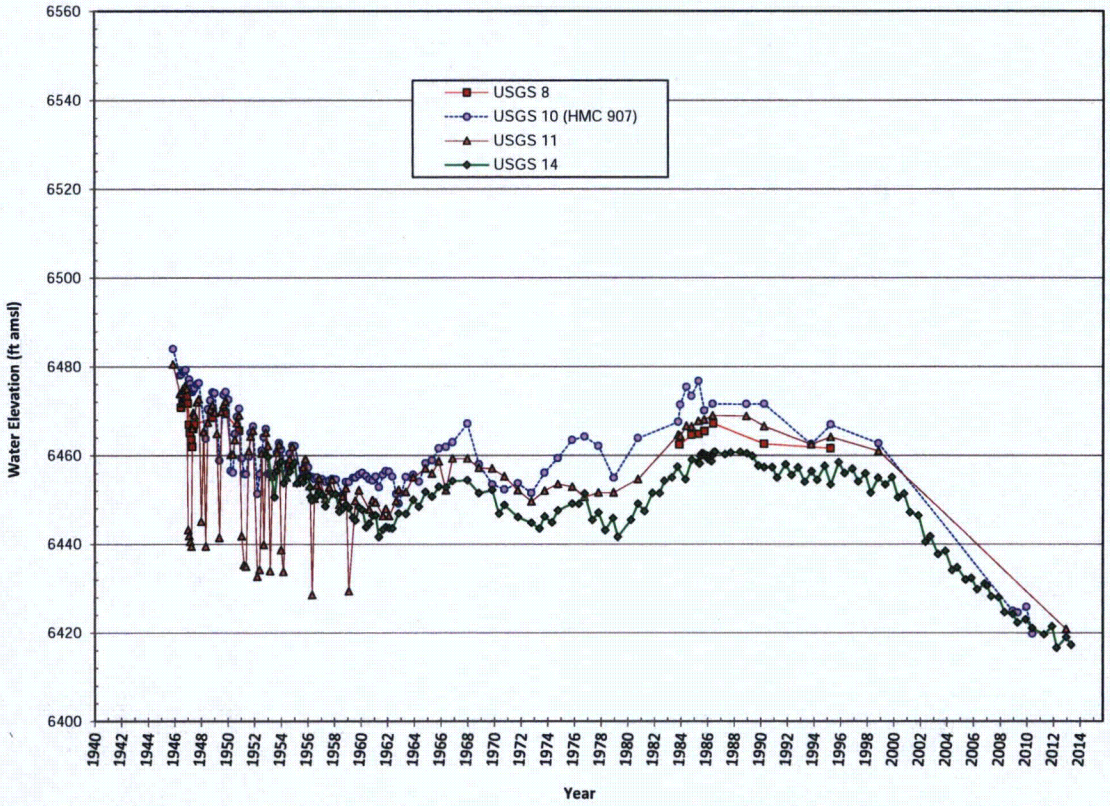

Figure 29. Hydrographs for USGS Wells Screened in the San Andres Aquifer in the South Valley Area

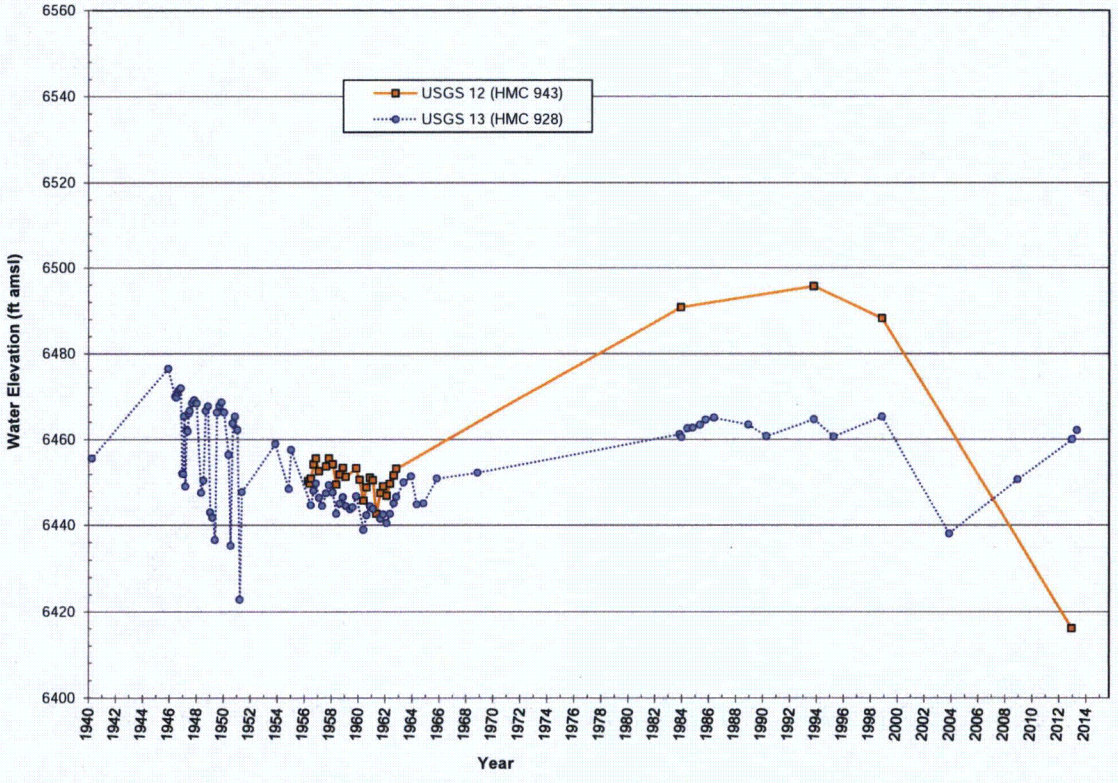

Figure 30. Hydrographs for USGS Wells Screened in the San Andres Aquifer near the Homestake Site

The reason for an increase in hydraulic head at USGS well 12 of about 40 ft between the early 1960s and the mid-1990s is unclear. As with USGS well 13, it is possible that the groundwater remedy at the GRP, which produces a downward gradient and potential downward flow between the alluvial aquifer and the San Andres aquifer played a role in the observed increase in the 1990s. However, the reason hydraulic head at USGS 12 increased in the mid-1980s, prior to implementation of the groundwater remedy, is not understood.

In contrast to the numerous wells monitored in the San Andres aquifer, USGS monitored historical hydraulic heads at only two wells that could be considered representative of the alluvial aquifer within the study area. Figure 31 shows the hydrograph for an alluvial aquifer well about 1 mi north of Milan (USGS 11) and another hydrograph for a well screened in Bluewater Basalt (USGS 5), about 1 mile west of the main tailings disposal cell at the Bluewater site. The ranges in measured hydraulic head at these monitoring locations over the past 65 years are limited to about 20 to 30 ft, as opposed to 50 to 70 ft in the San Andres aquifer wells. Though these two hydrographs are not necessarily representative of the Grants-Bluewater Valley in general, they do suggest that water level variations in the alluvial aquifer are moderated by groundwater responding to hydraulic stresses (e.g., pumping, recharge) under water table conditions. In contrast, hydraulic heads in the San Andres aquifer respond to hydrologic stresses under confined conditions, which reflect the effects of formation compressibility and minor water compressibility. It is likely that recharge of the alluvial aquifer by infiltration of precipitation, streambed seepage, irrigation canal losses, and application of irrigation water to the land surface has helped to minimize water level declines in the aquifer during dry years and periods of heavy regional pumping. Also, the ancestral Rio San Jose alluvium at the Bluewater site ranges from about 0 to 25 ft thick, thus limiting the potential variation in hydraulic head to about 25 ft in that area.

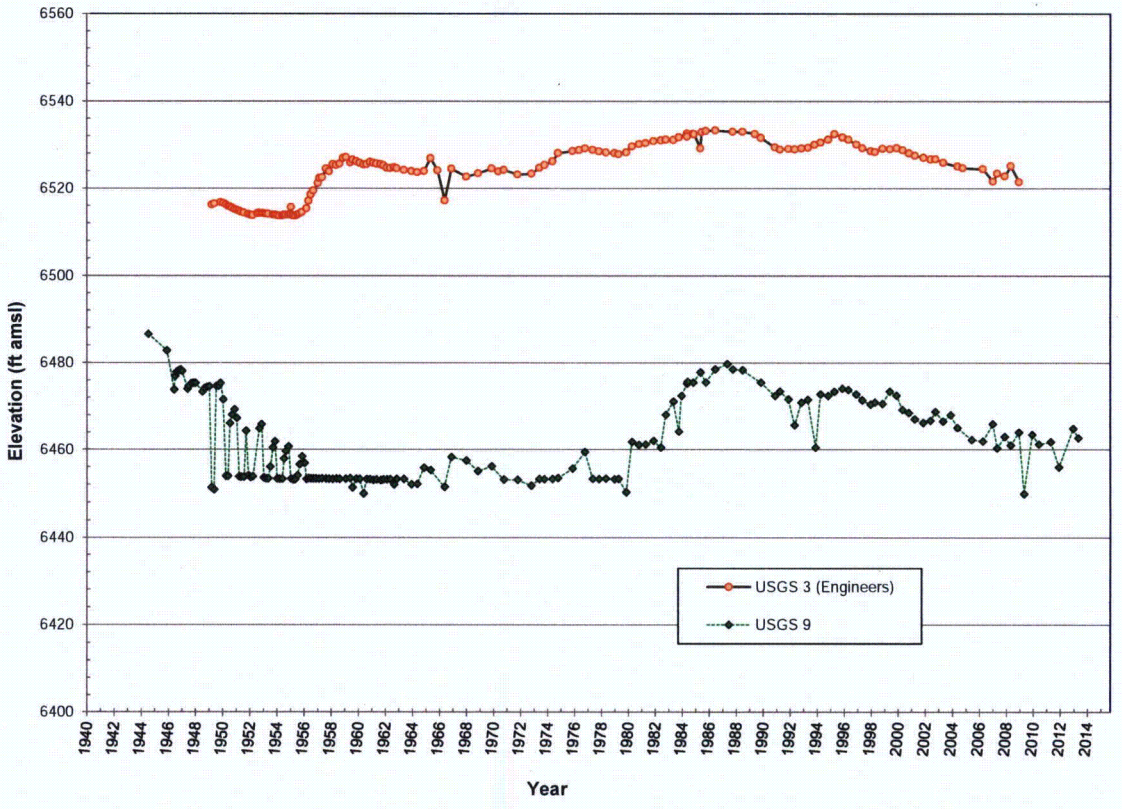

Figure 31. Hydrographs for USGS Wells Screened in the Alluvial Aquifer and the Bluewater Basalt

This page intentionally left blank

5.0 Regional Water Chemistry

This chapter discusses the background chemistry of water resources in the study area. Background water chemistry is considered important because it can influence whether a contaminant stays in solution. In addition, background water chemistry affects the chemical form of the contaminant as it is transported from contaminant sources to downgradient monitoring wells. Much of this chapter focuses on aqueous chemical parameters that influence the transport and retardation properties of uranium, the main contaminant of concern. The chemistry of major ions dissolved in regional water resources is also discussed, partly because it can be used for characterizing the chemical signatures of water in different aqueous environments.

The transport and retardation properties of uranium are typically influenced by the pH, bicarbonate concentration, and oxidation potential of an aqueous system. Uranium is mobile in the oxidized U(VI) state and becomes immobile if chemically reduced to U(IV). Bicarbonate ions complex with U(VI), favoring partitioning into the dissolved, mobile phase. U(VI) is least mobile at near-neutral pH with low bicarbonate concentration. At pH values less than about 4.5, and at pH values above 8 with elevated bicarbonate, U(VI) is most mobile. U(VI) immobility is often caused by its adsorption to mineral particles, particularly hydrous iron oxides. Clay minerals can also adsorb U(VI), but quartz, feldspar, and other major silicate minerals are less adsorptive. Since adsorption is an interaction with mineral surfaces, minerals with high surface area (e.g., clays and iron oxyhydroxide) are more adsorptive than those with low surface area (e.g., quartz).

As previously mentioned, major ion chemistry can be examined for chemical signatures that help distinguish one aqueous environment from another. Changes in major ion chemistry are also useful for constraining mass transfers between the mobile aqueous phase and immobile mineral phases. For example, if water samples are collected at two locations along a known flow path, the change in chemistry can be used to determine the chemical processes (e.g., ion exchange, adsorption, mineral precipitation, mixing) that might have occurred to account for the changes.

Mineral saturation indexes in regional water resources are also calculated in this chapter using the geochemical speciation program PHREEQC (Parkhurst and Appelo 2013). The saturation indexes of calcite ($CaCO_3$) and gypsum ($CaSO_4 \cdot 2H_2O$) provide information on aquifer-mineral interactions.

Data used in this chapter are presented in tabular and graphical forms. Abbreviations are used to denote waters from specific media. The abbreviation "Qb" denotes groundwater in basalt. "SA" denotes groundwater samples collected from wells screened in the San Andres aquifer, and additional abbreviations are used to identify whether each San Andres aquifer well is specifically screened in Glorieta Sandstone (GSS) only or San Andres Limestone (SAL) only. "Qal" signifies groundwater from wells screened in the alluvial aquifer, and "SW" is used to identify surface water chemistry.

5.1 Surface Water

The quality of surface water in the region is useful for understanding the chemical nature of groundwater recharge caused by seepage losses from streams and other surface water bodies. Because surface water is scarce within the region, data from only four background sampling

locations (SW-01 through SW-04) were found to support this analysis, and all of the locations are outside and hydraulically upgradient of the study area. Sampling dates for the four surface water locations varied from 1980 to 2010.

Two surface water sites are in the Bluewater Creek drainage, with one location at Bluewater Lake and the other on the creek itself. The chemistry at these sites is significant because they collectively constitute a major recharge source for both the alluvial and San Andres aquifers upgradient of the Bluewater site. Groundwater fed by this recharge flows beneath the Bluewater site and mobilizes remnant contamination in the subsurface. The remaining two surface water locations are in the San Mateo Creek drainage (Figure 32), several miles northeast of the Homestake site. The water chemistries at these latter locations are not representative of infrequent floodwaters in San Mateo Creek that reach as far south as the Homestake site. However, they do represent the chemistry of recharge water for the San Mateo Creek alluvium upgradient of the Homestake site.

Although stagnant areas of streams or lakes can produce reducing conditions, it is likely that most of the flowing streams in the area are oxidized, and any uranium in them would be in the U(VI) oxidation state. In fresh water, dissolved oxygen (DO) concentrations in equilibrium with the atmosphere range from about 7.5 mg/L at 30 °C to 12.8 mg/L at 5 °C (Hem 1986). DO concentrations, measured on three of the four samples collected from surface water, were 7.83, 9.84, and 13.8 mg/L, consistent with oxidized conditions (Table 6).

High iron concentrations generally indicate reduced conditions in natural groundwater, because oxidized iron readily forms low-solubility minerals. The oxidation state for a particular iron concentration is dependent on many solution parameters. Generally, iron concentrations less than about 0.05 mg/L are likely to represent oxidation states higher than the stability field for reduced uranium minerals. Because iron is a common rock-forming mineral, it can be easily included in a groundwater sample as a colloid or particulate. In these cases, an elevated iron concentration does not provide information about oxidation state. Dissolved iron concentrations were measured in three surface water samples with results of 0.004, 0.052, and 0.068 mg/L, values likely representing oxidized conditions.

The pH values for the surface water samples were slightly basic, ranging from 7.80 to 8.70 (Table 6). Specific conductivity values, ranging from 134 to 500 microsiemens per centimeter (µS/cm), indicated relatively low to moderate salinity in these samples. The higher specific conductivity value of the Bluewater Lake sample (SW-02) may indicate evaporation effects.

Most of the major ion concentrations in the surface water samples are relatively low (Table 7), with bicarbonate dominating the anion composition (Figure 33a). The sample collected from Bluewater Creek (SW-01) had chemistry similar to that of Bluewater Lake but was more dilute than the lake sample (SW-02). Cations in Bluewater Lake and Bluewater Creek are dominated by calcium. In contrast, sodium accounts for approximately half of the cation equivalents in San Mateo Creek (SW-03) and El Rito Creek (SW-04) samples in the San Mateo Creek drainage.

The surface water samples are near saturation with calcite, as indicated by saturation indexes near zero (Figure 35). These indexes indicate that the surface water has dissolved calcite from the rocks in the region. All surface water samples are undersaturated (large negative saturation indexes) with gypsum, indicating less interaction with gypsum. Gypsum would be dissolved in these waters.

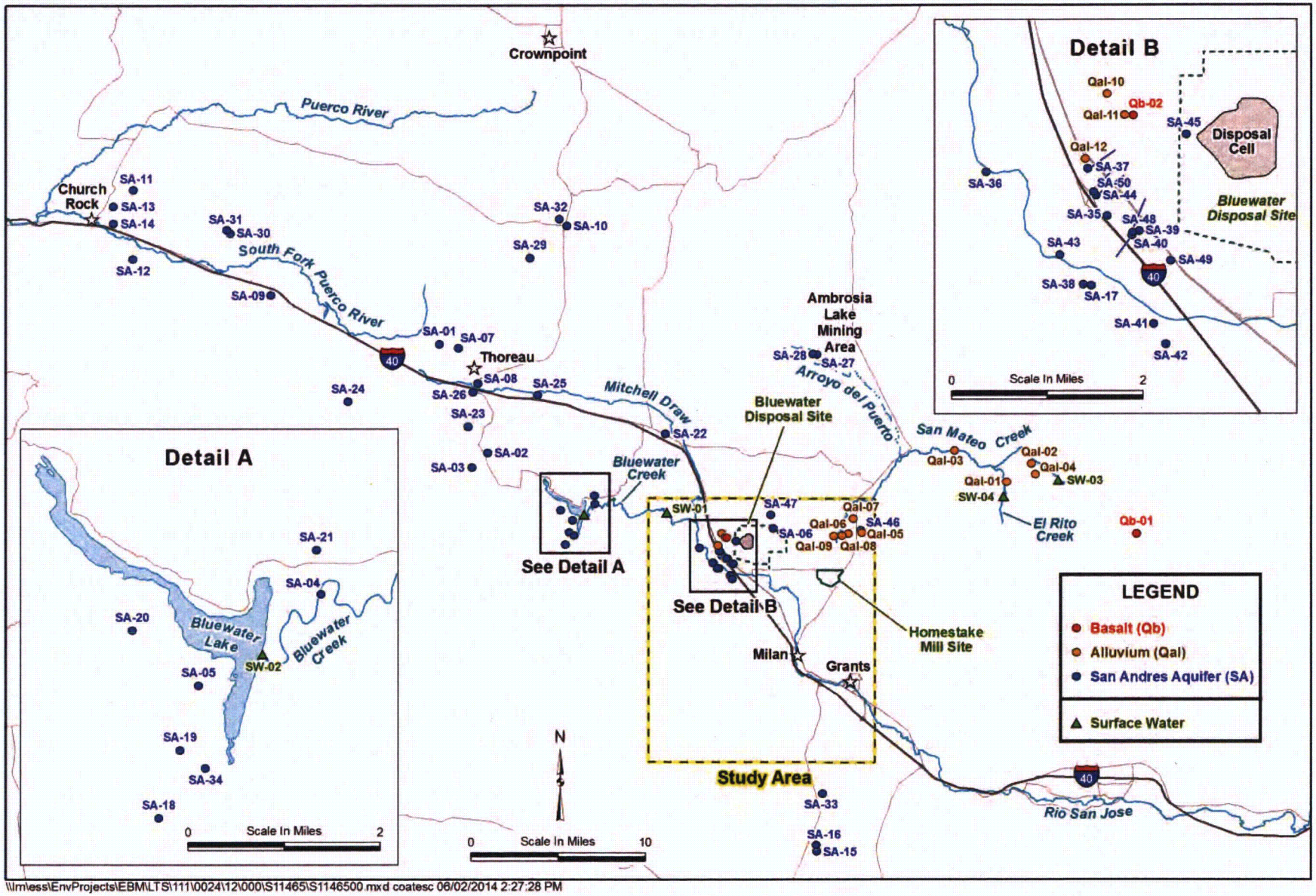

\\lrnless\EnvProjects\EBM\LTS\111\0024\12\000\S11465\S1146500.mxd coatesc 06/02/2014 2:27:28 PM

Figure 32. Background Sample Locations

Table 6. Field Parameters

Sample Identifier	Type	Source of Data	Date Sampled	Temperature (°C)	Dissolved Oxygen (mg/L)	pE[a]	pH	Specific Conductivity (µS/cm)
SW-01	SW	USGS	4/18/1980	6			7.80	310
SW-02	SW	USGS	2/19/1992	10	13.6		8.70	500
SW-03	SW	Lang	May-2010	15.8	7.83		8.09	134
SW-04	SW	Lang	May-2010	5.4	9.84		8.19	178
Qb-01	GW	B&R	8/29/1962	7.0			6.60	257
Qb-02[b]	GW	USGS	6/7/1957	19			7.50	1020
Qal-01	GW	Lang	8/21/2008				7.00	
Qal-02	GW	Lang	11/17/2008				7.50	
Qal-03	GW	Lang	2/18/2009				9.30	
Qal-04	GW	Lang	10/24/1961				8.00	
Qal-05	GW	NMED	3/30/2009	12.98	0.16	0.08	7.94	2341
Qal-06	GW	NMED	3/31/2009	13.05	0.2	7.19	6.92	3590
Qal-07	GW	NMED	3/31/2009	12.43	4.1	7.10	7.70	3206
Qal-08	GW	NMED	4/2/2009	13.52	1.52	3.77	6.83	2922
Qal-09	GW	NMED	4/2/2009	11.8	0.17	−0.40	8.76	1643
Qal-10	GW	DOE	4/11/1988	14			7.41	1050
Qal-11[b]	GW	DOE	4/11/1988	14			7.59	1020
Qal-12	GW	DOE	4/11/1988	14			7.24	1150
SA-01 (GSS-01)	GW	B&A	7/14/1970				8.50	1000
SA-02 (GSS-02)	GW	B&A	7/25/1986	12.5			7.48	725
SA-03 (GSS-03)	GW	B&A	12/11/1962	11.5			8.00	476
SA-04 (GSS-04)	GW	B&A	8/17/1963	13			7.60	770
SA-05 (GSS-05)	GW	B&A	8/19/1962				7.40	755
SA-06 (GSS-06)	GW	B&A	4/22/1959	24			7.20	4360
SA-07 (SAL-01)	GW	Lang	7/14/1970				8.50	
SA-08 (SAL-02)	GW	Lang	3/13/1975				7.30	

Table 6 (continued). Field Parameters

Sample Identifier	Type	Source of Data	Date Sampled	Temperature (°C)	Dissolved Oxygen (mg/L)	pE[a]	pH	Specific Conductivity (µS/cm)
SA-09 (SAL-03)	GW	Lang	7/19/1961				7.40	
SA-10 (SAL-04)	GW	Lang	1/26/1975				7.70	
SA-11 (SAL-05)	GW	Lang	3/16/1972				7.90	
SA-12(SAL-06)	GW	Lang	3/23/1972				8.40	
SA-13 (SAL-07)	GW	Lang	10/2/1968				7.30	
SA-14 (SAL-08)	GW	Lang	1/1/1967				8.20	
SA-15	GW	B&A	3/5/1986	15.5			7.40	420
SA-16	GW	B&A	3/5/1986	16.0			7.26	575
SA-17	GW	B&A	3/10/1965				7.20	1460
SA-18	GW	B&A	8/30/1964				7.40	647
SA-19	GW	B&A	8/19/1962				7.20	1110
SA-20	GW	B&A	8/9/1962	16.0			7.40	1390
SA-21	GW	B&A	9/4/1962	13.0			7.80	1120
SA-22	GW	B&A	3/7/1986	18.5			7.10	1330
SA-23	GW	B&A	7/19/1961	17.0			7.30	529
SA-24	GW	B&A	5/29/1963				7.30	490
SA-25	GW	B&A	8/20/1963	19.5			7.70	903
SA-26	GW	B&A	7/19/1961	19.0			7.40	563
SA-27	GW	B&A	8/8/1962	20.5			7.40	1030
SA-28	GW	B&A	3/5/1986	40.0			6.50	2850
SA-29	GW	B&A	2/24/1982	20.0			7.40	470
SA-30	GW	B&A	3/16/1972				7.90	1170
SA-31	GW	B&A	6/22/1955	15.5			7.30	1190
SA-32	GW	B&A	12/6/1975				7.70	960
SA-33	GW	B&R	10/13/1964	17.0			7.40	1180

Table 6 (continued). Field Parameters

Sample Identifier	Type	Source of Data	Date Sampled	Temperature (°C)	Dissolved Oxygen (mg/L)	pE[a]	pH	Specific Conductivity (µS/cm)
SA-34	GW	B&R	8/30/1964				7.40	647
SA-35	GW	NMED	8/25/2008	18.51	1.98	5.52	6.69	1613
SA-36	GW	NMED	8/26/2008	15.29	1.84	6.09	6.34	3231
SA-37	GW	NMED	8/26/2008	14.9	4.86	5.54	6.98	847
SA-38	GW	NMED	8/26/2008	13.94	15.87	5.90	6.66	1068
SA-39	GW	NMED	8/26/2008	14.43	9.67	6.33	6.55	962
SA-40	GW	NMED	8/26/2008	14.58	8.62	6.50	6.55	910
SA-41	GW	NMED	8/27/2008	13.52	3.9	6.22	6.84	1474
SA-42	GW	NMED	8/27/2008	13.67	3.89	6.90	6.82	1446
SA-43	GW	NMED	8/27/2008	15.01	5.32	5.83	6.58	1688
SA-44	GW	NMED	8/25/2008	15.42	1.53	5.70	6.72	2101
SA-45	GW	NMED	8/27/2008	17.16	0.81	−0.57	10.2	1344
SA-46	GW	NMED	8/25/2008	22.99	3.8	4.52	8.48	3857
SA-47	GW	DOE	4/4/1988	18			7.15	2800
SA-48	GW	DOE	4/11/1988	14			7.02	1050
SA-49	GW	DOE	4/11/1988	14			7.23	850
SA-50	GW	DOE	4/11/1988	16			6.94	2000

B&A = Baldwin and Anderholm (1992); B&R = Baldwin and Rankin (1995); DOE = DOE's environmental database; GSS = Glorieta Sandstone; GW = groundwater; Lang = Langman et al. (2012); µS/cm = microsiemens per centimeter; NMED = NMED (2010); Qal = Quaternary alluvium; Qb = basalt; SA = San Andres aquifer; SAL = San Andres Limestone; SW = surface water; USGS = USGS (2014)

[a] pE values based on measured oxidation-reduction potential.
[b] Samples Qb-02 and Qal-11 are probably from the same well. USGS considers sample Qb-02 to be from a well screened in Bluewater Basalt, whereas others investigating the Bluewater site (e.g., Hydro-Search [1977, 1981a]; Dames & Moore [1986b]) have traditionally considered a well at the same location to be an alluvial aquifer well known as Engineers.

Table 7. Major Ion Concentrations (mg/L)

Location	Calcium	Magnesium	Sodium	Potassium	Chloride	Bicarbonate	Carbonate	Sulfate
SW-01	47	9.4	5.5	1.7	2.2	98.9	0.22	50
SW-02	79	18	10	2.9	5.7	146	0	150
SW-03	10	2.8	9.8	3.7	2.2	76.6	0.40	2.6
SW-04	16	4.4	12	3.8	2.7	101.7	0.51	2
Qb-01	26	6.1	6.2	1.4	45	33.2	0.0	5.2
Qb-02[a]								
Qal-01	54	16	78	1.0	7	312.3	0.19	22
Qal-02	71	17	264	2.0	34	473.4	1.02	264
Qal-03	10	4	313	4.0	34	399.3	53.97	273
Qal-04	10	2.4	10	3.0	1.6	65.8	0.35	1
Qal-05	567	149	261	7	47	186.3	1.04	2110
Qal-06	479	88.5	269	10.1	55	173.2	0.09	1580
Qal-07	59	10.3	628	0.5	125	240.2	0.68	955
Qal-08	389	73.7	355	8.4	59	159.8	0.07	1610
Qal-09	4.94	0.84	434	1.1	58	286.9	8.44	535
Qal-10	130	37	57	5	41	242.3	0.32	296
Qal-11[a]	130	34	66	6	42	267.3	0.54	299
Qal-12	170	40	26	6	57	248.0	0.23	325
SA-01 (GSS-01)	31	14	170	0	150	208.4	4.17	72
SA-02 (GSS-02)	62	20	79	1.7	6.5	254.3	0.36	150
SA-03 (GSS-03)	76	14	8	0.9	9.6	256.4	1.11	33
SA-04 (GSS-04)	100	37	12	0	8	211.0	0.40	220
SA-05 (GSS-05)	110	35	8.1	1	14	260.3	0.42	170
SA-06 (GSS-06)	600	140	430	0	300	243.0	0.33	2200
SA-07 (SAL-01)	31	14	170		150	208.4	4.17	72
SA-08 (SAL-02)	150	28	11	1.8	4.8	156.0	0.20	350

Table 7 (continued). Major Ion Concentrations (mg/L)

Location	Calcium	Magnesium	Sodium	Potassium	Chloride	Bicarbonate	Carbonate	Sulfate
SA-09 (SAL-03)	90	15	10	1.2	4.8	252.7	0.39	72
SA-10 (SAL-04)	54	18	130		1.8	169.5	0.55	300
SA-11 (SAL-05)	190	37	25		9.9	222.2	1.21	460
SA-12(SAL-06)	170	82	27	5.0	6.4	171.0	3.01	590
SA-13 (SAL-07)	260	59	1100	21.0	63	97.4	0.18	3000
SA-14 (SAL-08)	120	15	200	3.0	23	188.5	2.09	610
SA-15	39	13	37	2.8	14	193.7	0.23	19
SA-16	52	18	40	3.3	19	231.1	0.21	48
SA-17	180	48	88		69	309.0	0.34	400
SA-18	82	29	14	1.0	13	261.3	0.41	87
SA-19	180	48	9.9	1.0	12	257.3	0.28	390
SA-20	260	45	12		13	264.6	0.38	580
SA-21	160	60	20	2.0	8.1	259.1	0.84	420
SA-22	180	76	40	3.1	3.8	188.7	0.15	680
SA-23	78	19	9.5	0.8	8.0	228.5	0.23	63
SA-24	67	14	20	1.0	4.6	231.2	0.28	48
SA-25	120	38	23		4.8	231.7	0.67	290
SA-26	90	15	10	1.2	4.8	251.6	0.34	72
SA-27	73	33	120		15	288.6	0.43	280
SA-28	260	79	370	14	240	367.8	0.12	1000
SA-29	50	18	13	2.9	2.9	171.7	0.23	84
SA-30	190	37	25		9.9	222.2	1.21	460
SA-31	180	55	14		6.0	208.4	0.23	490
SA-32	54	18	130		1.8	169.5	0.55	300
SA-33	120	41	75	5	80	267.7	0.38	270

Table 7 (continued). Major Ion Concentrations (mg/L)

Location	Calcium	Magnesium	Sodium	Potassium	Chloride	Bicarbonate	Carbonate	Sulfate
SA-34	82	29	14	1	13	261.3	0.41	87
SA-35	170	52.7	178	6.32	101	295.7	0.09	475
SA-36	422	96.1	420	13.7	262	287.0	0.04	1440
SA-37	138	35.2	37.3	3.38	25	238.5	0.12	245
SA-38	164	43.3	71.1	5.46	40	231.4	0.06	345
SA-39	165	35.3	34.9	2.69	17	241.6	0.04	241
SA-40	147	33.6	26.5	2.97	14	225.1	0.04	222
SA-41	143	47	95.7	7.83	45	256.1	0.09	352
SA-42	149	44.8	83.7	6.1	39	251.4	0.09	342
SA-43	196	59.4	56.1	3.99	48	211.7	0.04	451
SA-44	167	53.5	191	5.34	107	302.4	0.09	478
SA-45	0.6	1.9	332	5.47	217	110.4	98.14	2.5
SA-46	159	47.1	106	6.19	65	299.1	6.03	434
SA-47	200	62	350	14	236	586.9	0.54	666
SA-48	170	31	43	2	21	352.4	0.19	242
SA-49	120	31	38	4	30	227.0	0.19	228
SA-50	190	58	190	5	158	293.9	0.15	574

GSS = Glorieta Sandstone; mg/L = milligrams per liter; Qal = Quaternary alluvium; Qb = basalt; SA = San Andres aquifer; SAL = San Andres Limestone; SW = surface water

[a] Samples Qb-02 and Qal-11 are probably from the same well. USGS considers Qb-02 to be from a well screened in basalt, whereas others investigating the Bluewater site (e.g., Hydro-Search [1977, 1981a]; Dames & Moore [1986b]) have traditionally considered a well at the same location to be an alluvial aquifer well known as Engineers.

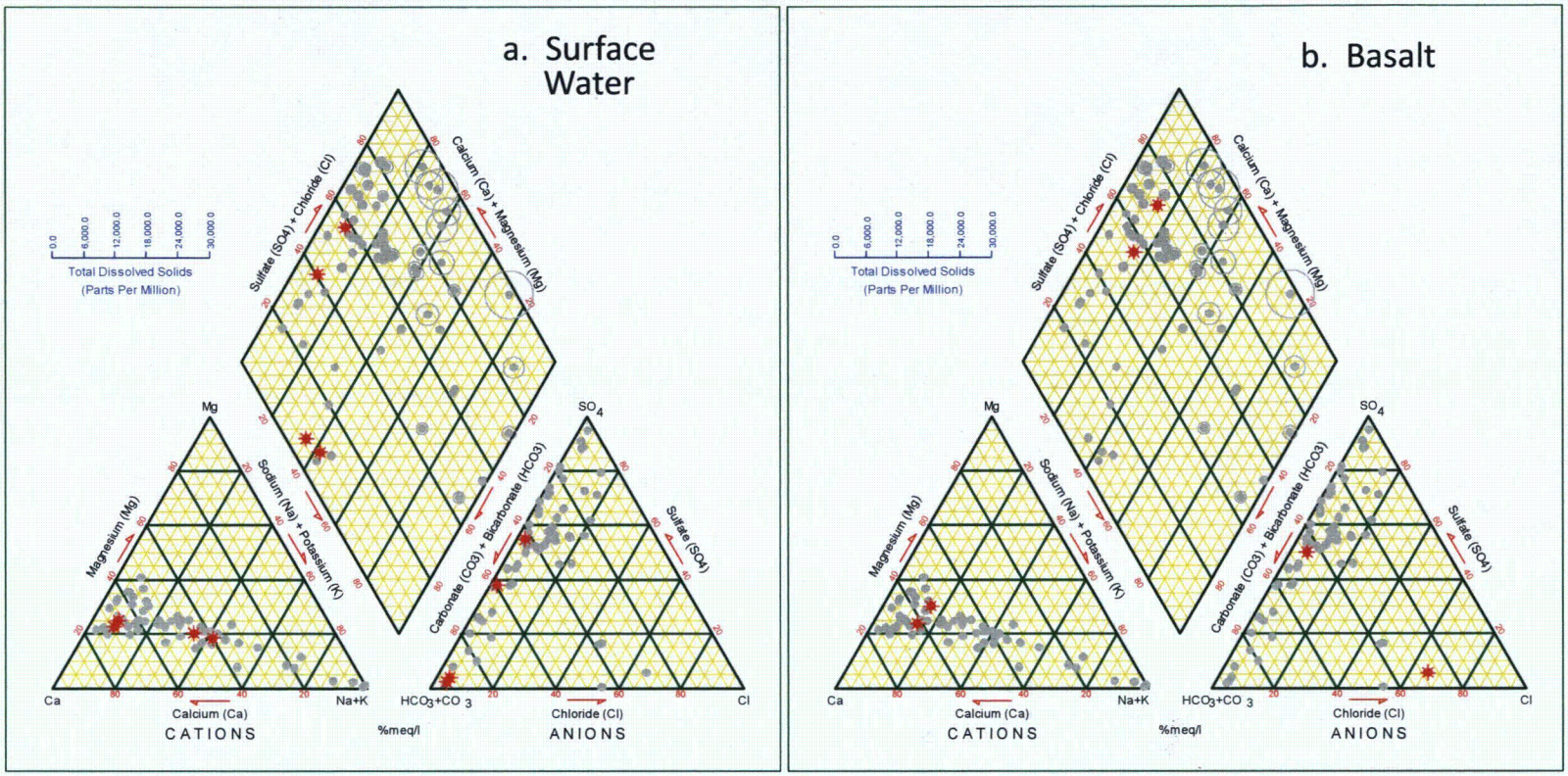

Figure 33. Piper Diagrams for (a) Surface Water and (b) Basalt Background Samples
(Gray symbols are the complete set of background samples used in this study. Red symbols are the designated subgroups.)

Data on contaminant concentrations in surface water were available only from San Mateo Creek and El Rito Creek samples. Arsenic, molybdenum, and selenium concentrations were less than their respective detection limits, and uranium concentrations were less than 0.001 mg/L. These results suggest that surface watercourses in the San Mateo Creek drainage are not receiving high fluxes of these contaminants from natural sources.

5.2 Hydrogeologic Units

5.2.1 Quaternary Alluvium

Concentrations of dissolved constituents in alluvial aquifer groundwater samples from 12 wells were found in three different information sources (Table 6). Locations Qal-01 through Qal-09 are in San Mateo Creek alluvium, with Qal-l through Qal-04 in the upper reaches of the creek drainage and Qal-05 through Qal-09 in the area directly north of the Homestake large tailings disposal cell. Locations Qal-10 through Qal-12 are in the Rio San Jose drainage, about 1 mi west of the Bluewater site main tailings disposal cell.

Oxidation states were measured on five of the alluvial groundwater samples. These were reported as values of pE, which is a dimensionless quantity defined as the negative logarithm (to the base 10) of the electron activity in a solution; the larger the pE value, the more oxidized the solution. The pE results indicated that oxidation states in the alluvial aquifer are variable. However, most water samples collected at alluvial aquifer wells are relatively oxidized, such that reduced uranium minerals would not precipitate even in the sample with the lowest oxidation state (pE = −0.40). There are difficulties in getting measurements of oxidation state representative of in situ conditions. Oxygenation of samples prior to or during measurements of DO can affect results. DO concentrations are consistent with variable oxidation states and generally correlate with pE values. Even the lowest DO concentration of 0.16 mg/L would correlate to a pE value of more than 12.

Dissolved iron concentrations were measured in nine alluvial aquifer samples. Iron concentrations were relatively low, ranging from 0.020 to 0.080 mg/L, consistent with oxidized conditions.

Cation equivalents in the alluvial groundwater are dominated by sodium and calcium, with less than 30 percent magnesium (Figure 34a). The samples from the recent and ancestral Rio San Jose alluvium have higher calcium and lower sodium equivalents than those from the San Mateo Creek alluvium. Anions in the alluvial groundwater are dominated by bicarbonate and sulfate with relatively low equivalents of chloride (Figure 34a). The samples from Rio San Jose alluvium are nearly equivalent in bicarbonate and sulfate. Samples collected from alluvium near the upper reaches of San Mateo Creek are dominated by bicarbonate, whereas those from alluvium directly north of the Homestake site are dominated by sulfate. The anion distribution for groundwater from alluvium in the upper San Mateo Creek drainage suggests that the groundwater is derived from seepage through carbonate-rich bedrock, while the alluvium associated with the reach of the creek north of the Homestake site is more likely representative of surface water infiltrating and seeping through gypsiferous soils or contaminated soils. Contaminated soils in the San Mateo Creek drainage in areas north of the Homestake site are generally attributed to mining and milling activities in the Ambrosia Lake Valley.

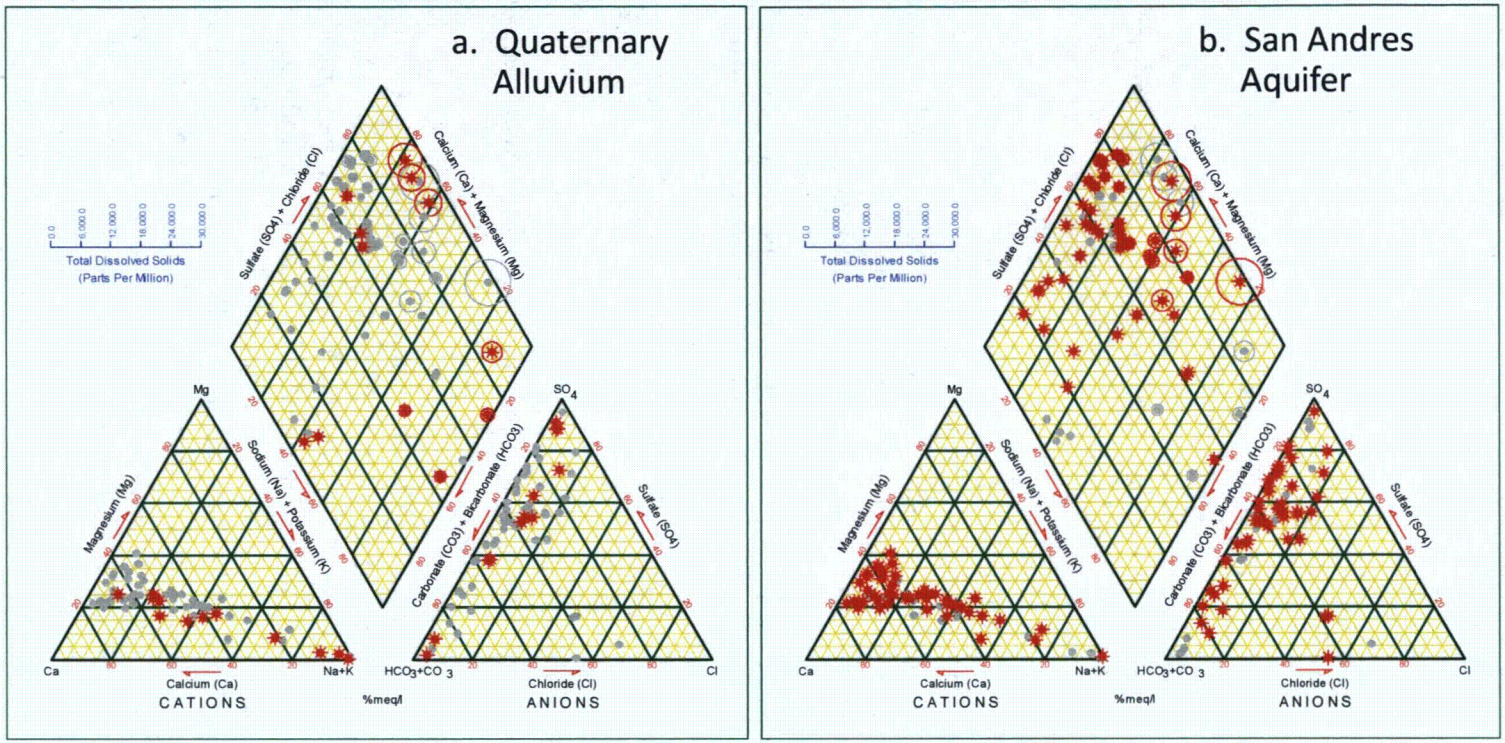

Figure 34. Piper Diagrams for (a) Quaternary Alluvium and (b) San Andres Aquifer Background Samples (Gray symbols are the complete set of background samples used in this study. Red symbols are the designated subgroups.)

Many of the alluvial groundwater samples are oversaturated with calcite, and the rest are only slightly undersaturated (Figure 35). The saturation indexes suggest that groundwater in alluvium is in contact with calcite, likely derived from abundant limestone in the region. Samples Qal-05, Qal-06, and Qal-08, which are from San Mateo Creek alluvium north of the Homestake site, have the highest salinities, as indicated by the specific conductivities for these locations (Table 6). These three samples also have the highest gypsum saturation indexes (Figure 35), supporting the possible origin of infiltration and seepage through gypsiferous soils.

Alluvial groundwater samples from the San Mateo Creek alluvium north of the Homestake site had elevated concentrations of uranium, with three of the five samples showing uranium concentrations greater than 0.1 mg/L. The three samples with elevated uranium also had selenium concentrations exceeding 0.3 mg/L. These results indicate that alluvial groundwater in this area is contaminated, presumably due to an influx of contaminated waters derived from mining activity in Ambrosia Lake Valley.

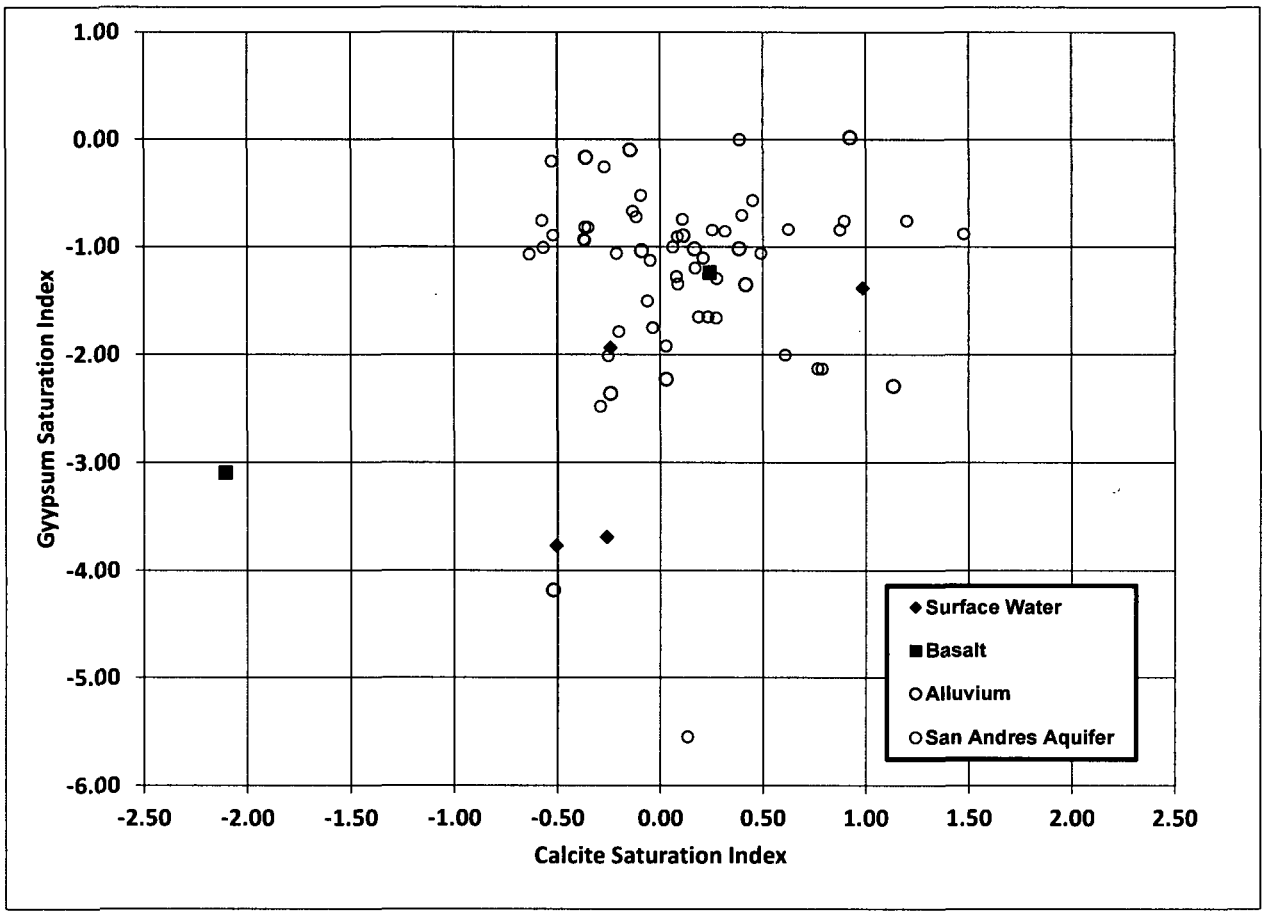

Figure 35. Saturation Indexes for Calcite and Gypsum in Background Samples

5.2.2 Basalts

Groundwater chemistry data from only two wells completed in basalt were located for this analysis. Sample Qb-01 is from basalt in the San Mateo Mountains, and Qb-02 is from Bluewater Basalt about 0.6 mi west of the main tailings disposal cell (Figure 32). No oxidation-

Bluewater Basalt about 0.6 mi west of the main tailings disposal cell (Figure 32). No oxidation-reduction values were available for these waters; however, the groundwater was likely oxidized, based on the shallow depth of each well and a lack of reduced solid matter in these rocks. One sample was analyzed for iron with a result of 0.05 mg/L, consistent with oxidized conditions.

Recharge of water in mountains above the Qb-01 location resulted in low salinity (specific conductivity) and a calcium-chloride composition (Figure 33b). The sample from the Bluewater Basalt had higher salinity, similar cation composition, but an anion composition dominated by sulfate and bicarbonate rather than chloride.

5.2.3 Chinle Formation

Limited data are available regarding the chemistry of groundwater in the Chinle Formation. As a consequence, no specific chemical data for Chinle Formation wells are reported in Table 6 and Table 7. Instead, a brief description of the water chemistry in the Chinle Formation is presented here based on information presented in Baldwin and Anderholm (1992) and Baldwin and Rankin (1995).

Groundwater in the Chinle Formation is generally a sodium-bicarbonate or a sodium-bicarbonate-sulfate water that has small calcium and chloride percentages. The increased sodium concentrations in the Chinle Formation groundwater are probably due to ion-exchange reactions that occur in interbedded shales and clays. Water from wells screened in the Chinle Formation tends to have relatively large TDS concentrations, reflecting long residence times. TDS levels vary from approximately 500 to about 18,000 mg/L. This wide range reflects the complex and highly varied nature of flow systems in Chinle Formation strata. In contrast to the alluvial and San Andres aquifers in the study area, sodium concentrations in Chinle Formation groundwater typically account for 83 to 97 percent of total cations (Baldwin and Rankin 1995).

5.2.4 San Andres Aquifer

Groundwater chemistry in the geologic formations of the San Andres aquifer (San Andres Limestone and Glorieta Sandstone) is largely controlled by lithologies represented in these formations. The dominant lithology is sandstone that contains calcareous cement (mostly calcite with dolomite) and fine-grained pyrite. Most of the pyrite is presumably in fine-grained sandstone found near the top of the San Andres Limestone, as observed in the vicinity of the Bluewater site (Section 3.3.2.4). In addition, beds of gypsum and anhydrite are in the sandstone-dominated formations (Baldwin and Rankin 1995).

Background groundwater chemistry data for the San Andres aquifer are available from the USGS study by Baldwin and Anderholm (1992), specifically for an area near the town of Thoreau, which is located about 19 mi northwest of the Bluewater site. According to Baldwin and Anderholm (1992), the chemistry of the groundwater in the San Andres aquifer is less variable in the Thoreau area than in the Bluewater area.

The presence of pyrite in sandstones of the San Andres aquifer suggests that groundwater in the aquifer may occur under a low oxidation state. However, all pE values for 12 water samples collected from the aquifer were greater than 5, indicating that much of the groundwater in the aquifer is oxidized. Low concentrations of dissolved iron were also observed in most of the

samples, consistent with oxidized conditions. Four groundwater samples from wells screened in the San Andres aquifer had iron concentrations exceeding 1 mg/L. These high iron concentrations could be representative of localized reduced conditions, or the water containing the high iron levels may have been compromised by inadvertent incorporation of particulate iron during sampling. The mineral uraninite is about 6 orders-of-magnitude undersaturated in the San Andres aquifer samples, including in the sample with the lowest pE, which suggests relatively oxidized conditions.

Specific conductivity values in the San Andres aquifer are mostly less than 1,000 µS/cm, indicating moderately high salinity. As indicated in Figure 34b, cation chemistry in most of the San Andres aquifer samples is dominated by calcium, while a few of the samples are dominated by sodium. This variation between calcium dominance in some locations and sodium dominance in others might be the result of cation exchange processes in the aquifer. Anions are spread between bicarbonate and sulfate with little chloride. Molar ratios of bicarbonate to sulfate range from about 1 to 12, with most ratios around 5. The samples with the highest concentrations of dissolved solids are typically high in sulfate. All San Andres aquifer samples were undersaturated with gypsum, indicating that the groundwater has a tendency to dissolve gypsum (Figure 35). Gypsum dissolution is a potential cause of the high salinity in bedrock groundwater. The San Andres aquifer samples are mostly near saturation with calcite, but saturation levels span a broad range from −0.64 to 1.48, reflecting varying amounts of water interaction with carbonate minerals.

Twelve samples of San Andres aquifer groundwater had analytical results for contaminants. In all 12 samples, molybdenum concentrations were less than the instrument detection limit for this constituent. The samples were also low in uranium and nitrate, with the highest-concentration samples showing about 0.011 mg/L uranium and 10.9 mg/L nitrate (as NO_3).

5.3 Background Uranium Concentration

Detailed information regarding the background concentrations of uranium in the alluvial and San Andres aquifers would be beneficial for evaluating the spatial extent of uranium contamination in groundwater due to milling activity in the Grants-Bluewater Valley. Unfortunately, no detailed quantitative assessment of background concentrations for this constituent has ever been conducted. This problem stems from a variety of issues, including (1) a scarcity of dissolved uranium concentration data for wells installed in uncontaminated portions of the two aquifers; (2) the fact that groundwater quality tends to degrade with flow distance and, therefore, residence time in each aquifer; (3) local natural variations in water quality; and (4) leakage of lower-quality water from adjacent formations (e.g., Chinle Formation, Yeso Formation). Nonetheless, a report to ARCO by Applied Hydrology Associates, Inc. (1990) aimed at selecting a corrective action program and establishing alternate concentration limits for selected contaminants at the Bluewater site provides data from which useful approximations of background uranium concentration can be deduced.

Using water chemistry data for samples collected from wells E(M), Aragon, Berryhill House, and Engineers (see Figure 16 and Plate 7), Applied Hydrology Associates, Inc. (1990) reported that the background uranium concentration in the alluvial aquifer varied from 0.003 to 0.04 mg/L. Similarly, concentration data from bedrock wells Bowlins, L(SG), M(SG), and Berryhill Section 5 were used to identify a background uranium concentration range of 0.003 to

0.013 mg/L for the San Andres aquifer. With these findings, Applied Hydrology Associates, Inc. (1990) concluded that there was no significant difference in background uranium concentration between the two aquifers.

On the basis of the above-mentioned concentration ranges, it is assumed in this study that a uranium concentration of 0.01 mg/L is representative of background conditions in both aquifers. Though slightly lower and higher concentrations could probably be identified in uncontaminated wells in the Grants-Bluewater Valley, this value appears reasonable for preliminarily assessing the spatial extent of the uranium plumes in the two aquifers. As discussed in later chapters, a concentration of 0.01 mg/L is used in this report to delineate the lateral boundaries and the leading edge of the uranium plumes emanating from the Bluewater site in the alluvial and San Andres aquifers. It is possible that additional chemical characterization methods (e.g., uranium isotope concentrations) would be helpful for identifying uranium contamination if concentrations slightly larger than 0.01 mg/L are measured at wells located far from the plumes originating at the Bluewater and Homestake sites.

6.0 Disposal Cell Performance

Most of the tailings generated during the 30-year history of milling operations were deposited in the main tailings impoundment. During site reclamation, this impoundment was enclosed with an engineered cover consisting of a clay layer and rock to prevent radon emissions and erosion of the encapsulated tailings (Figure 36). Seepage of tailings fluids from the tailings impoundment and subsequent disposal cell is addressed in this section.

Figure 36. Site Marker near the Southwest Corner of the Main Tailings Disposal Cell

6.1 Tailings Disposal History

Initial deposition of tailings in the main tailings impoundment began in 1956 in a basalt depression that was located in what is now the middle of the main tailings disposal cell. A limited quantity of carbonate tailings was deposited in this depression, followed thereafter by acidic tailings. After initial depositions began to fill the depression, a series of soil starter dikes were constructed to control the surface area of the pond. At this point, the footprint of the tailings pond covered not only basalt surfaces but also windblown sand deposits and an outcrop of San Andres Limestone.

Tailings were conveyed in a slurry and discharged continuously from three movable spigots along the south side of the impoundment. Coarser sands settled near the spigots, and mixed fine sand, silt, and clay settled in the middle portion of the impoundment, with silt and clay (referred to as "slimes") settling out in the north end, where tailings fluid formed a pond. Figure 37 shows the approximate distribution of these materials.

As tailings deposition continued, dikes were periodically raised to contain the tailings and tailings pond. By 1957, the main tailings impoundment attained a footprint similar to that of the final impoundment (and disposal cell). By 1981, the elevation on the south side was 56 ft higher than the north side because of the buildup of sand tailings in that area.

6.2 Main Tailings Impoundment Seepage

ARCO recognized that substantial quantities of tailings fluids seeped through the bottom of the main tailings impoundment, through the underlying unsaturated materials, and into the alluvial and San Andres aquifers. Various estimates of seepage losses through the bottom of the main tailings impoundment were made by Anaconda and ARCO hydrology subcontractors (Arlin et al. 1978, Dames & Moore 1984a, ARCO 1990, Applied Hydrology Associates Inc. 1995). All agreed that high seepage losses of at least 1,000 gpm occurred in the 1950s. To reduce the amount of seepage, Anaconda constructed a deep injection well in 1960.

The injection well, located more than a mile northeast of the tailings impoundment (Figure 4), was completed in the Yeso Formation that underlies the Glorieta Sandstone. Tailings fluid decanted from the pond that persisted at the north (lowest elevation) end of the main tailings impoundment was injected into the well from 1960 through 1977. The injection rate was regulated to ensure only gravity flow within the well (i.e., injection was not under pressure). Approximately 501 million gallons of decanted fluid had been injected by the end of 1965 (West 1972), which is an average rate of approximately 190 gpm. Assuming this rate continued, a total of approximately 1.7 billion gallons of decanted fluids were injected during the operation of the well. In their evaluation of the Bluewater site injection process, USGS considered it to be the most satisfactory and economically feasible method of effluent disposal (West 1972).

After 1977, tailings fluids were evaporated in lined evaporation ponds constructed north of the impoundment. Use of the evaporation ponds removed approximately 525 million gallons of liquid that otherwise would have infiltrated into the tailings. During the years 1977 through 1982, much of the uranium in the decanted water was recovered by recycling the evaporation pond water through the mill (ARCO 1995).

Ore-milling operations and tailings deposition ceased in March 1982. Subsequently, ARCO installed 58 extraction wells in the sand portion of the tailings impoundment. These wells removed approximately 122 million gallons of interstitial fluids from the tailings as part of a program to dewater the impoundment and recover uranium. The extracted fluids were treated at the mill, and most of the barren solution was pumped to the evaporation ponds. The remaining unreported amount of treated water was sprayed on the tailings for dust control during interim tailings impoundment stabilization activities. Pumping from these wells ceased in 1985 when water levels and well yields dropped to levels at which pumping was no longer practical (ARCO 1995).

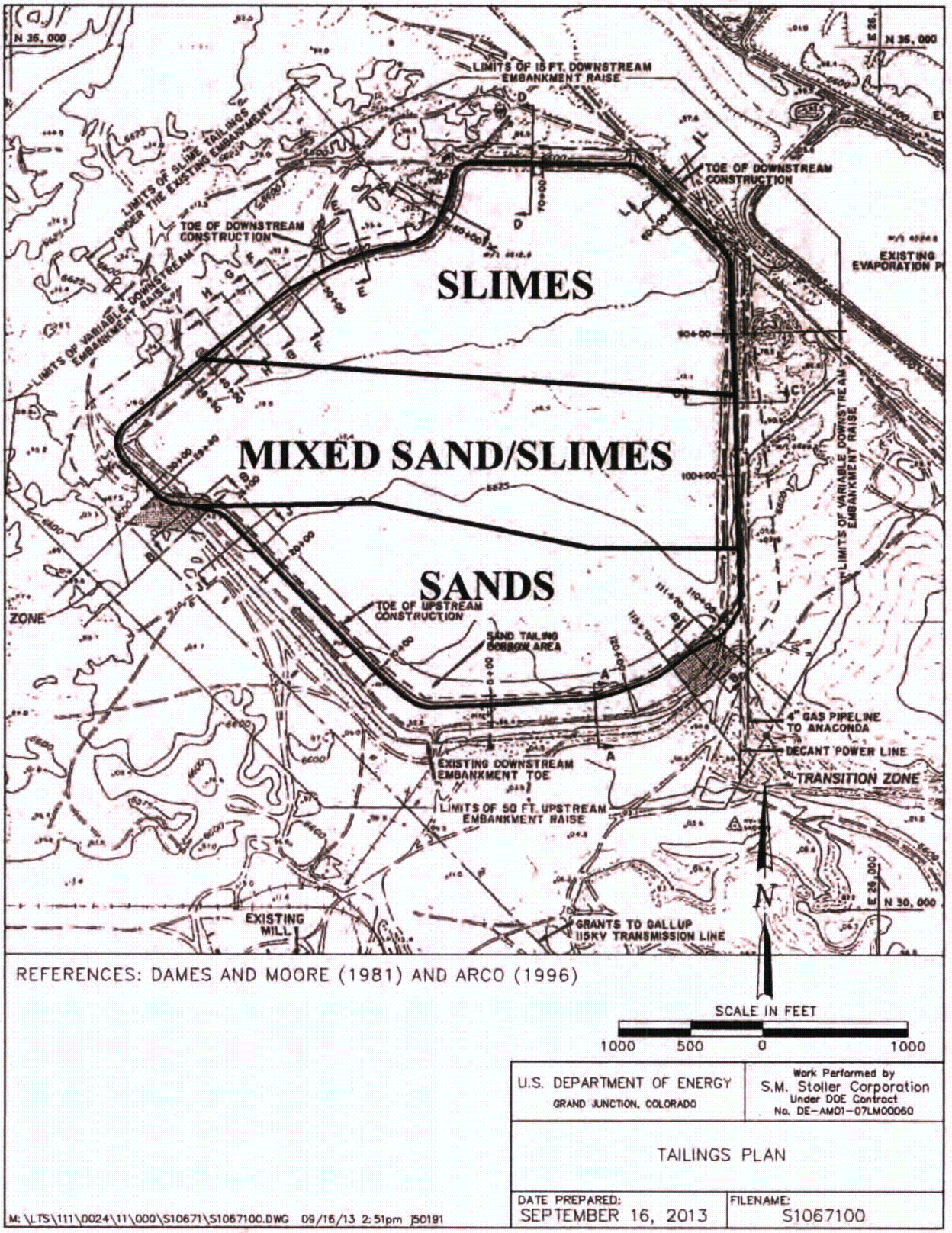

Figure 37. Approximate Distribution of Materials Within the Main Tailings Impoundment

Prior to placement of the radon barrier, ARCO installed vertical band drains to wick fluids out of the slimes. The purposes of this procedure were to reduce the quantity of tailings fluids available for seepage and to consolidate the slimes. Tailings were loaded with a consolidation layer of windblown silty and sandy clay materials (the same type of material used to construct the radon barrier) to squeeze fluid out of the slimes and into the drains.

The wicks drew approximately 24 million gallons of tailings fluids to the surface of the impoundment, where the fluids ponded and evaporated. ARCO calculated that up to 16 million gallons of fluids moved into unsaturated materials of the consolidation layer, thus removing a total of approximately 40 million gallons from potential seepage (Applied Hydrology Associates Inc. 1993). Approximately 7.4 million gallons of fluids were assumed to have been forced through the bottom of the impoundment during the consolidation process (derived from Appendix A, Table A-1). Monitoring results from wells adjacent to the impoundment, however, did not show any increase in contaminant concentrations in either the alluvial or San Andres aquifers as a result of this activity. The band drains were removed when 90 percent consolidation of the slimes had been attained and flow from the band drains ceased. The final cover materials (radon barrier and rock) were installed at that time.

Estimated seepage rates from the tailings impoundment into underlying materials and aquifers were based on mill water-balance calculations, including fluid discharge to the tailings impoundment, decantation of the ponded fluids to the injection well and later to the evaporation ponds, cell dewatering activities, tailings fluid reprocessing, and precipitation. However, ARCO did not account for evaporation of the tailings fluid and precipitation runoff that ponded at the north end of the impoundment prior to decantation activities; these processes may have essentially cancelled each other out, thus not significantly affecting ARCO's seepage rate calculations. Evaporation of the ponded fluids following the start of decantation for deep-well injection (and later disposal in the evaporation ponds) was assumed to have been minimal because most of the ponded water was decanted (Dames & Moore 1981a). A schematic of the Bluewater mill impoundment water cycle is shown in Figure 38.

Cumulative seepage rates from the main tailings impoundment, based on ARCO's last estimates (Applied Hydrology Associates Inc. 1995), are plotted in Figure 39. ARCO estimated that approximately 2.7 billion gallons of tailings fluid seeped from the main tailings impoundment by the time deep-well injection commenced in 1960. Thereafter, seepage continued at a reduced rate. By the time construction of the disposal cell and placement of the rock cover was completed in 1995, ARCO estimated that approximately 5.7 billion gallons of fluid had seeped through the bottom of the impoundment (Appendix A, Table A-1). Although evaporation of tailings pond fluid would have removed some water from the cycle, ARCO's estimate of 5.7 billion gallons of seeped fluid through 1995 is considered to be the best available estimate and is used in this assessment.

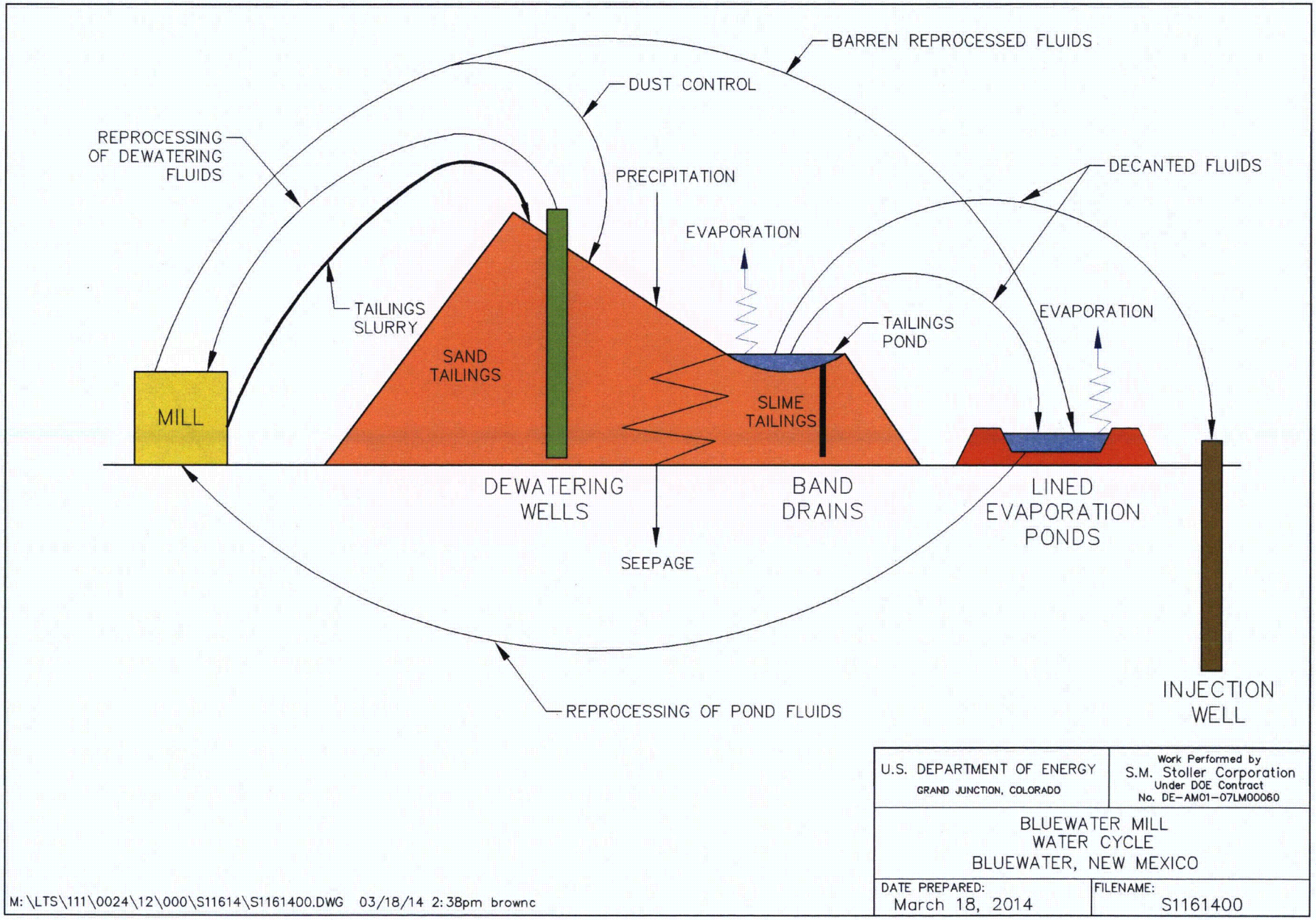

Figure 38. Schematic of the Tailings Impoundment Water Cycle

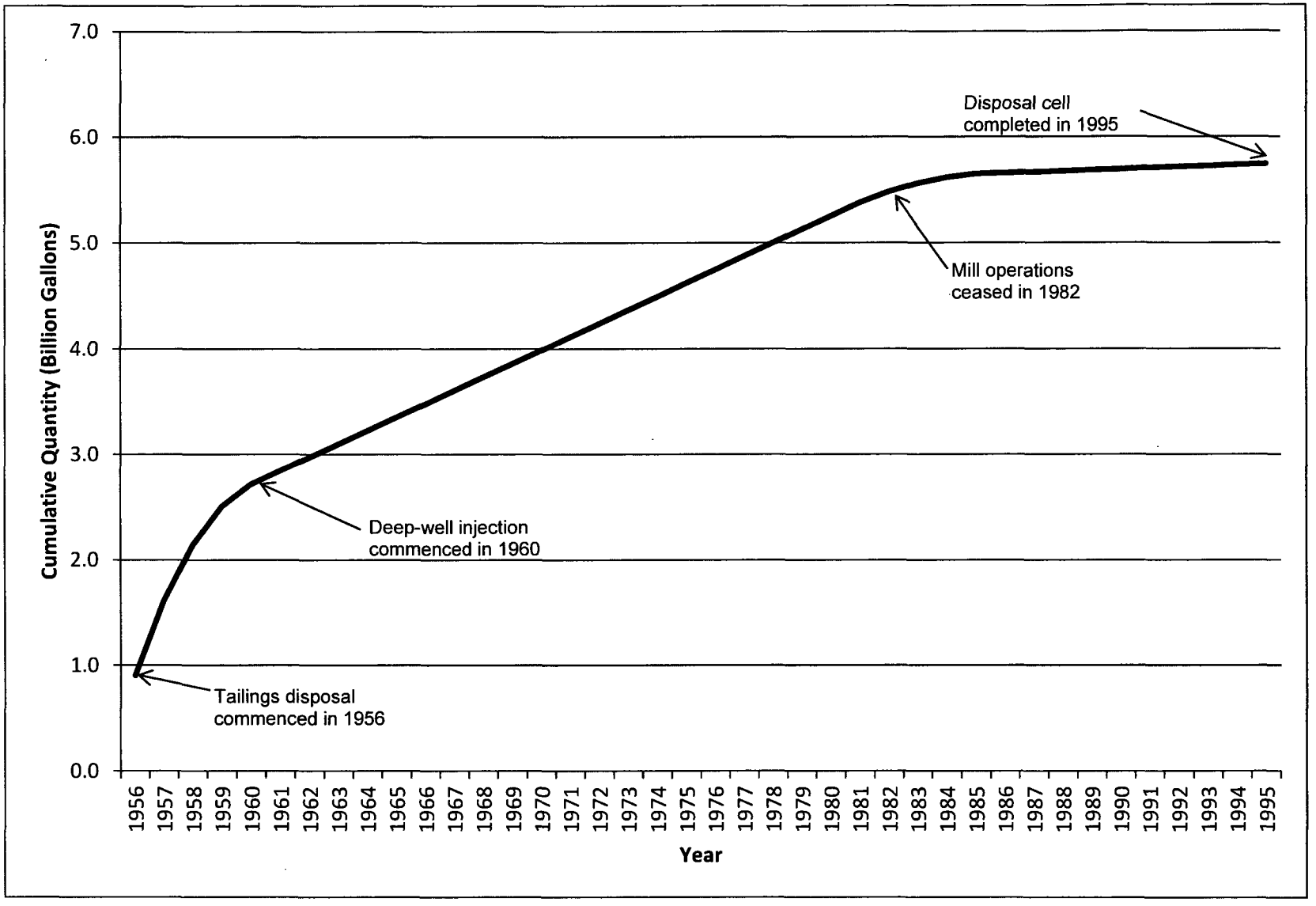

Figure 39. Estimated Cumulative Seepage from the Main Tailings Impoundment Through 1995

6.3 Disposal Cell Performance

A liner was not installed prior to tailings placement, and the tailings were encapsulated in place. Therefore, tailings fluids remaining in the disposal cell, and additional fluids from infiltration of precipitation through the cover, could continue to seep through the bottom of the disposal cell. This assumption of continuing seepage is considered to apply to other rock-covered UMTRCA disposal cells where the tailings were stabilized in place.

A key component of understanding how much fluid could seep out of the disposal cell is evaluating how much precipitation is entering the cell. Therefore, an understanding of how the disposal cell cover was designed and constructed, and how it may change over time, helps characterize the potential hydraulic performance of the cover.

6.3.1 Cell Cover Design and Construction

The main tailings disposal cell cover, completed in December 1995, was designed primarily to satisfy federal regulations and standards for radon attenuation and erosion protection as directed by UMTRCA. Federal regulations and NRC guidelines require groundwater protection but do not include standards or criteria for cover permeability or percolation. Nor was the potential for plant encroachment, root intrusion, or animal burrowing in the cover evaluated. The assumption, however, was that the engineered cover would prevent infiltration of precipitation into the encapsulated tailings, thus eventually eliminating the disposal cell as a continuing source of contamination (after seepage of residual fluids).

Designers used NRC guidelines to calculate radon barrier thicknesses for different surfaces of the main tailings disposal cell to limit radon flux, as required, to less than the 20 picocuries per square meter per second (pCi/m^2s) standard (Title 10 *Code of Federal Regulations* Part 40, Appendix A). The radon barrier, consisting of sandy-clay material from the site, ranged in thicknesses from 1.0 to 4.2 ft, with the greatest thickness over the sand tailings (ARCO 1996). Prior to placement of the radon barrier, the tailings surface was graded and covered by up to 15 ft of compacted relocated materials derived from natural windblown deposits and evaporation pond dike materials from the site (primarily sandy-clay material identical to the radon barrier material). The greatest thicknesses of relocated materials were placed over the slimes portion of the tailings, most of which were placed for dewatering through the band drains. Some of these materials contained low levels of windblown radioactive contamination.

The radon barrier was compacted to 100 percent of maximum dry density based on Standard Proctor density. As-built permeability values were not reported. However, a common construction assumption at the time was that laboratory permeability (saturated hydraulic conductivity [*Ks*]) results could be achieved in the field. Designers likely assumed, based on their laboratory results, that by compacting the radon barrier to 100 percent of Standard Proctor density, they had achieved an as-built permeability in the range of 1×10^{-7} to 1×10^{-8} centimeters per second (cm/s).

NRC guidelines (NRC 1990) were used to calculate runoff discharge and velocity from the top and side slopes of the cell and the size of basalt rock necessary to control erosion of these slopes. The NRC procedure is based on calculations of the probable maximum precipitation event and resulting probable maximum flood event.

Cover slopes were designed to shed runoff water primarily to the north. However, the north top slope was designed at a 0.5 percent slope, leaving little latitude for construction irregularities or settlement. The final constructed surface in this area had a 0.45 percent slope (ARCO 1996). The as-built surface topography and cross sections of the main tailings disposal cell are shown in Appendix A, Figures B-2 through B-4.

The condition of vegetation along the north toe slope indicates that runoff is not shedding off of the north edge of the cover as intended. If runoff was occurring, more abundant plant growth would be present along the flat north toe slope where runoff water would accumulate. However, plant growth along the north toe slope appears to be no greater than in surrounding areas, and moist areas have not been observed in this area.

6.3.2 Existing Conditions of the Cell Cover

Depressions have formed on the north end of the disposal cell cover, which is over the portion of the cell containing slimes. These depressions collect runoff water after storm events of sufficient magnitude or intensity (Figure 40). They were first observed by DOE inspectors during the first annual inspection in 1998. Satellite imagery taken in 1997 verifies that they had already started developing before DOE acquired the site. The depressions apparently formed as the slimes continued to consolidate after completion of the cover, which occurred soon after removal of the band drains.

In 2012, DOE conducted a high-resolution topographic survey of the main tailings disposal cell using a light detection and ranging (LiDAR) method to provide a baseline to determine if differential settlement in the depression area is ongoing (DOE intends to conduct another LiDAR survey in 2015). No standing water was present on the cover at the time of the survey. The digital LiDAR survey data were used to develop 6-inch contour intervals for the disposal cell surfaces (Appendix A, Figure 9) and to calculate the areas, depths, and volumes of the depressions. Based on light-colored evaporite minerals that form as ponded water evaporates from the depressions and corresponding elevations determined by the survey, the maximum ponded area has been approximately 15.3 acres. The maximum depth of ponded water has been 2.5 ft in the deepest depression, and the maximum quantity of ponded water has been approximately 4.3 million gallons (Appendix A, Figure 10). This maximum ponded area appears to have occurred during spring 2012 following melting of unusually high snowfall amounts during the previous December. No significant precipitation occurred during the spring, but standing water persisted until mid-June.

Observations of differential settlement and ponding of water have raised concerns about water percolation through the cover, leaching of tailings constituents, and the stability of the north end of the disposal cell. Field observations of the persistence of ponded water suggest that most of it dissipates by evaporation rather than percolation through the cover. Evapotranspiration plays an insignificant role on this portion of the cover because very little vegetation is present.

Figure 40. Ponds in Depressions on the Main Tailings Disposal Cell in August 2012, Following a Summer Storm Event

To determine if the depressions are having an adverse effect on the performance of the radon barrier, radon flux measurements were collected on the uncovered surface of the radon barrier over the area encompassing the depressions (Appendix A, Figure 11). The measurements were collected in early July 2013, after a dry spring and prior to the annual monsoon season; no ponded water was present on the cover. The cell cover materials were at their driest condition of the year, which would be when the highest radon emissions would be expected to occur. Moisture attenuates radon, so radon emission would not occur through wet materials or standing water. A typical measurement location is shown in Figure 41.

Figure 41. Radon Measurement Location RF-05 in the Area of Cell Cover Depressions

Radon flux was below the laboratory detection limit of 0.5 pCi/m^2s at all of the locations (the design limit is 20 pCi/m^2s). These results suggest that the deformation of the cover in this area has not opened pathways (i.e., cracks or soil fissures through the radon barrier) for radon emission from the underlying tailings materials; therefore, the radon barrier is performing as designed. These results may also imply that the permeability of the radon barrier has not increased by development of the depressions and associated deformation of the surface, or by any other changes that may have occurred since the cover was constructed.